EUROPEAN ORGANIZATION FOR NUCLEAR RESEARCH

CERN-EP/85-171
22 October 1985

STUDY OF $\eta\pi^+\pi^-$ STATES IN THE $\rho'(1600)$ MASS REGION PHOTOPRODUCED IN THE REACTION $\gamma p \to \eta\pi^+\pi^- p$ AT PHOTON ENERGIES OF 20 TO 70 GeV

Omega Photon Collaboration

M. Atkinson[7], T.J. Axon[5], D. Barberis[5], T.J. Brodbeck[4], G.R. Brookes[8], J.J. Bunn[8], P.J. Bussey[3], A.B. Clegg[4], J.B. Dainton[3], M. Davenport[7], B. Dickinson[5], B. Diekmann[1], A. Donnachie[5], R.J. Ellison[5], P. Flower[7], P.J. Flynn[4], W. Galbraith[8], K. Heinloth[1], R.C.W. Henderson[4], R.E. Hughes-Jones[5], J.S. Hutton[7], M. Ibbotson[5], H.-P. Jakob[1], M. Jung[1], B.R. Kumar[7], J. Laberrigue[6], G.D. Lafferty[5], J.B. Lane[5], J.-C. Lassalle[2], J.M. Lévy[6], V. Liebenau[1], H. Marsiske[1], R.H. McClatchey[8], D. Mercer[5], J.A.G. Morris[7], J.V. Morris[7], D. Newton[4], C. Paterson[3], G.N. Patrick[2], E. Paul[1], C. Raine[3], M. Reidenbach[1], H. Rotscheidt[1], A. Schlösser[1], P.H. Sharp[7], I.O. Skillicorn[3], K.M. Smith[3], K.M. Storr[2], R.J. Thompson[5], Ch. de la Vaissière[6], A.P. Waite[5], M.F. Worsell[5] and T.P. Yiou[6]

Bonn[1]-CERN[2]-Glasgow[3]-Lancaster[4]-Manchester[5]-Paris VI[6]-Rutherford[7]-Sheffield[8]

ABSTRACT

In diffractive photoproduction of $\eta\pi^+\pi^-$, the two-body substates $\eta\rho^0$ and $A_2\pi$ are found to contribute significantly to the cross-section for $\eta\pi^+\pi^-$ masses below 2.4 GeV. From a spin-parity analysis the branching ratio, $\rho'(1600) \to \eta\rho/\rho'(1600) \to$ all, is determined to be < 0.02 at the 68.3% confidence level. The $A_2\pi$ component shows an enhancement around 1.7 GeV. The spin-parity analysis indicates a probable contribution to this signal from exclusive photoproduction of the g(1690).

(To be submitted to Zeitschrift für Physik C)

0027P/EP/sm

1. INTRODUCTION

The $\rho'(1600)$ is the best established candidate for a radial excitation of a vector meson composed of light quarks. It has been observed in the decay modes $\rho^{o}\pi^{+}\pi^{-}$ [1,2], $\rho^{\pm}\pi^{\mp}\pi^{o}$ [3,4] and $\pi^{+}\pi^{-}$ [5]. In both an earlier photoproduction experiment [6] and $e^{+}e^{-}$ annihilation [7] there is some evidence for an enhancement in the $\eta\pi^{+}\pi^{-}$ mass spectrum in the $\rho'(1600)$ mass range but no detailed analysis has yet been done due mainly to poor statistics.

In this paper a detailed study of the reaction

$$\gamma p \rightarrow \eta\pi^{+}\pi^{-}p \qquad (1)$$

is presented allowing a search for the decay modes $\rho'(1600) \rightarrow \eta\pi^{+}\pi^{-}$ via the substates $\eta\rho^{o}$, $A_2\pi$, and $\delta\pi$. The data come from a general study of photoproduction of hadrons by photons of energy 20-70 GeV. The experiment (WA57) was performed using the Omega Spectrometer at the CERN SPS. A previous analysis of reaction (1) from this experiment has studied $\eta\pi^{+}\pi^{-}$ masses below 1.4 GeV [8]. The analysis presented here extends the mass range up to 2.4 GeV.

2. EXPERIMENT AND DATA SELECTION

A description of the experiment and details of the trigger and the data selection can be found in the previous publication on reaction (1) [8] and are therefore not reported here. The final data sample for the present analysis of reaction (1) was obtained by requiring that the events had a $\gamma\gamma$ pair with effective mass between 0.50 and 0.59 GeV (see Fig. 1) and that the missing energy, ΔE, to the incident photon and $\eta\pi^{+}\pi^{-}$ system was within the range -1.5 to +2.5 GeV (see Fig. 2). With these selections a final sample of 1871 events corresponding to reaction (1) was obtained. In order to calculate the acceptance of the events in the experimental set-up, reaction (1) was simulated by a Monte-Carlo program [9]. The photon bremsstrahlung spectrum was generated according to the experimental spectrum. The production cross-section was taken to be independent of photon energy and the differential cross-section $d\sigma/dt$ was taken as exponential with a slope of 5 GeV^{-2}. The

$\eta\pi^+\pi^-$ mass distribution was generated with a shape similar to the experimental one and the $\eta\pi^+\pi^-$ system was allowed to decay according to Lorentz-invariant phase space. The normal to the $\eta\pi^+\pi^-$ decay plane was distributed isotropically. The events were passed through an acceptance program [10] which simulated the experimental conditions including the multiplicity requirement of the trigger, the geometrical cuts imposed by the apparatus and the inefficiencies of the chambers. In addition this program included a full simulation of showering in the photon detector and reconstruction of γ rays. A bin-by-bin division of the spectra for accepted events by those for generated events then yielded the acceptance as a function of all relevant kinematical variables for the analysis described below.

3. RESULTS

3.1 Reaction cross-sections and mass spectra

The $\gamma\gamma$ mass spectrum was fitted to a Gaussian distribution plus a second-order polynomial background giving for the peak:

$$m = (545.3 \pm 0.7)\ \text{MeV}$$

$$\Gamma = (20.2 \pm 0.6)\ \text{MeV}\ .$$

The width is consistent with the experimental resolution. The background within the mass cut, 0.50 to 0.59 GeV, used to define the $\eta\pi^+\pi^-$ events for the present analysis is given by the fit as 22.5 ± 1.3%.

Figure 2 shows the missing energy distribution for events of reaction (1) deduced by a peak minus wings subtraction on the $\gamma\gamma$ mass spectrum (the wing regions were chosen to be $0.455 < m_{\gamma\gamma} < 0.500$ GeV and $0.590 < m_{\gamma\gamma} < 0.635$ GeV). The background from events with additional unobserved particles within the ΔE cut, -1.5 GeV to +2.5 GeV, is estimated to be 20 ± 10%. Figure 3 shows the raw distribution of the invariant $\eta\pi^+\pi^-$ mass obtained using this ΔE cut together with the peak minus wings subtraction on the $\gamma\gamma$ spectrum. The curve shows the overall acceptance.

For all the remaining analysis the background under the η peak (Fig. 1) has not been subtracted. Combining this background with that from inelastic contamination of the true $\eta\pi^+\pi^-$ events (Fig. 2), the

total background is estimated to be 35 ± 10% of the final event sample obtained with the selections described in Section 2.

Using the total luminosity for this experiment of 143 nb^{-1}, the overall acceptance weight of 10.7 for reaction (1) and a BR ($\eta \to \gamma\gamma$) of 0.39, the cross-section after correction for background and averaged over the incident photon energy range was determined to be

$$\sigma(\gamma p \to \eta\pi^+\pi^- p) = (234 \pm 6 \pm 50)\ nb$$

for $\eta\pi^+\pi^-$ masses up to 3.5 GeV. The errors are statistical and systematic, respectively.

The differential cross-section $d\sigma/dt$ has been fitted to an exponential distribution, $d\sigma/dt = e^{bt}$, as a function of incident photon energy and also of $\eta\pi^+\pi^-$ mass. The mean value of b was 4.8 ± 0.1 GeV and there was no significant variation of the shape with either photon energy or $\eta\pi^+\pi^-$ mass.

Figure 4a shows the acceptance-corrected $\eta\pi^\pm$ mass distribution for all selected events of reaction (1). The peak at ~ 1300 MeV is consistent with the $A_2(1320)$ which is the only well-established resonance at this mass with an $\eta\pi^\pm$ decay mode. There are also indications for $\delta(980) \to \eta\pi^\pm$, but this contributes only 3% to the total event sample and could be due to inelastic background [11]. For subsequent analysis the small δ signal was neglected. The $A_2(1320)$ was measured by fitting the $\eta\pi^\pm$ mass distribution using a relativistic Breit-Wigner peak with fixed mass and mass-dependent width [13] multiplied by a term of the form $(m_{A2}/m_{\eta\pi})^n$ [12] to account for the distortion of phase space by threshold effects. The background was represented by an exponential function of the form $\exp(a\, m_{\eta\pi} + b\, m^2_{\eta\pi})$.

Figure 4b shows such a fit for the total event sample (χ^2/ND = 10.9/10; n = 8 ± 3) and the signal corresponds to a 17 ± 2% A_2 contribution, representing a cross-section corrected for branching ratio of $A_2 \to \eta\pi$ = (14.5 ± 1.2)% of

$$\sigma(\gamma p \to A_2^{\pm}\pi^{+}\pi^{-}p) = 425 \pm 44 \pm 50 \text{ nb} .$$

Fits were also carried out for 100 MeV slices of the $\eta\pi^{+}\pi^{-}$ mass. The results are shown in Fig. 5.

Figure 6a shows the acceptance-corrected $\pi^{+}\pi^{-}$ mass distribution. The ρ^{o} intensity was determined by a fit using a Breit-Wigner form with fixed mass and mass-dependent width [13] plus a polynomial background. The Breit-Wigner peak was again multiplied by a term $(m_{\rho}/m_{\pi\pi})^{n}$ to allow for threshold effects causing skewing of the ρ^{o} shape. The result of the fit (χ^2/ND = 19/14; n = 6.0 ± 0.23) to the total mass spectrum is shown in Fig. 6b. 22 ± 2% of all events of reaction (1) have a ρ^{o}, corresponding to a cross-section $\sigma(\gamma p \to \eta\rho^{o}p)$ = 81 ± 6 ± 17 nb. Since the peak fitting procedure only worked down to an $\eta\pi^{+}\pi^{-}$ mass of about 1.4 GeV the cross-section represents possibly some underestimate. The ρ^{o} yield as a function of the $\eta\pi^{+}\pi^{-}$ mass is given in Fig. 7.

In the above cross-section determinations no correction has been applied for $A_2\pi$ and $\eta\rho$ production for events from the 35% background.

3.2 Decay angular distribution of the $\eta\pi^{+}\pi^{-}$ system

The decay angular distribution of the normal to the $\eta\pi^{+}\pi^{-}$ decay plane was studied after correction for acceptance losses both in the s-channel helicity system and in the Gottfried-Jackson system (t-channel helicity system). A selection of corresponding normalized spherical harmonic moments, $\langle Y_{\ell}^{m}\rangle$, for the s-channel analysis are shown in Fig. 8. All other moments in the s-channel helicity system and all in the Gottfried-Jackson system were found to be consistent with zero. The moment $\langle Y_2^{o}\rangle$ is expected to be the only nonvanishing moment for purely s-channel helicity conserving p-wave states [14]. This is found to hold in photoproduction of ρ^{o}, ω and ϕ mesons and is indicated in $\rho'(1600)$ production [1]. The $\eta\pi^{+}\pi^{-}$ data of Fig. 8 show no evidence for this effect in the $\rho'(1600)$ mass range.

3.3 Dalitz plot analysis

To analyse the spin parity of the $\eta\pi^+\pi^-$ system as a function of mass the method of maximum likelihood fits to the Dalitz plot was applied, with decay amplitudes constructed using the Zemach tensor formalism [15-17]. This analysis has the advantage that states with different spin parities do not interfere and that there is no dependence on the production mechanism of the $\eta\pi^+\pi^-$ system. Since the $\eta\pi^+\pi^-$ states contain substantial contributions from $A_2\pi$ and $\eta\rho^o$, both $A_2\pi$ and $\eta\rho^o$ decay amplitudes were constructed [18,19]. The different spin-parity states considered were: for $\eta\rho$, $J^P = 0^-, 1^-, 1^+, 2^+, 2^-$ and phase space; for $A_2\pi$, $J^P = 0^-, 1^+, 1^-, 2^+, 2^-, 3^-$ and phase space. The 1^+ $\eta\rho$ and 2^- $A_2\pi$ amplitudes can contain contributions from both S-wave and D-wave decay and these contributions may interfere. In practice, the fits were insensitive to the D/S wave ratio for both of these amplitudes and were unable to distinguish them from $\eta\rho$ and $A_2\pi$ phase space, respectively. Therefore, the 1^+ $\eta\rho$ and 2^- $A_2\pi$ amplitudes were not included in the final fits, but the corresponding contributions would be included in the $\eta\rho$ and $A_2\pi$ phase-space intensities. To allow for the presence of states other than $A_2\pi$ and $\eta\rho^o$ and particularly for background from reactions other than (1) an intensity corresponding to $\eta\pi^+\pi^-$ Lorentz invariant phase space was also included in the fits.

Given intensities I_{J^P}, the probability density function for event i is

$$f_i(\underset{\sim}{\alpha}) = \sum_{J^P} (\alpha_{J^P} I_{J^P}) / \int I_{J^P} \, dm_1^2 \, dm_2^2$$

where m_1 and m_2 are two out of the three possible two-particle mass combinations and α_{J^P} is the fraction of spin parity J^P in the data. Then the negative log-likelihood function to be minimized is

$$L(\underset{\sim}{\alpha}) = -\sum_i \log f_i(\underset{\sim}{\alpha})$$

with the summation over all events in a given interval of $\eta\pi^+\pi^-$ mass. The integrals over the Dalitz plot were performed by the Monte Carlo method using only simulated events (see Section 2) which fell within the acceptance aperture of the apparatus and were reconstructed by the

software. The same cuts were applied to both the data and the Monte Carlo events. The fits were made using the program MINUIT [20] in 200 MeV bins of $\eta\pi^+\pi^-$ mass.

In the initial fits all states listed previously were allowed to contribute. These fits were found to be poorly constrained, mainly due to the small event samples available in each mass bin. However, certain spin-parity contributions were consistently found to be zero within errors, and to constrain the fits further, these were fixed to zero. After various combinations of contributions had been tried, a subset consisting of 1^- $\eta\rho$, $\eta\rho$ phase space, 3^- $A_2\pi$, $A_2\pi$ phase space and $\eta\pi^+\pi^-$ phase space was found to be sufficient to obtain good fits to the data. Fits where any of these major contributions were removed or replaced by one of the other spin parities, always gave a value for the log-likelihood deviating significantly from the best fit. To illustrate these features, Table 1 gives the results of a variety of fits in the $\eta\pi^+\pi^-$ mass range 1.5-1.7 GeV.

The cross-sections for production of the various contributions as a function of $\eta\pi^+\pi^-$ mass, as obtained from the final fits, are given in Table 2 and in Fig. 9. The results of these fits have been investigated in terms of four variables: the $\eta\pi^\pm$ and $\pi^+\pi^-$ mass distributions and the angles $\theta_{A_2\pi}$ (the angle between the $\pi^\pm$ direction and the η direction in the $\eta\pi^\mp$ rest frame) and $\theta_{\eta\rho}$ (between the η and π^+ directions in the $\pi^+\pi^-$ rest frame). Distributions of these variables are given (open circles) in Figs. 10 to 13 as functions of $\eta\pi^+\pi^-$ mass: also shown (solid circles) are the distributions predicted by the fit results given in Table 2. All distributions show, in general, good agreement between the data and the Dalitz plot fit results.

Both the $A_2\pi$ and the $\eta\rho$ production cross-sections for the mass range $1.4 < m_{\eta\pi\pi} < 2.4$ GeV obtained from the Dalitz plot fits are slightly lower than those obtained from the fits to the mass spectra.

4. DISCUSSION OF RESULTS

Figure 9 shows the following features:

i) There is a substantial $J^P = 1^-$ contribution in the $\eta\rho^o$ system peaking at $\eta\rho^o$ threshold and falling with increasing mass.

ii) All three phase-space intensities ($\eta\rho^o$, $A_2\pi$, and $\eta\pi\pi$) contribute over the whole $\eta\pi\pi$ mass range and show no structure; these include $\eta\rho$ 1^+ S, $A_2\pi$ 2^- S and an appreciable contribution from background.

iii) There is a small $J^P = 3^-$ contribution to the $A_2\pi$ system peaking at a mass around 1.7 GeV.

The cross-section for production of $J^P = 1^-$ $\eta\rho^o$ in the $\rho'(1600)$ mass region (1.5 to 1.9 GeV) is measured to be 17 ± 7 ± 4 nb. This gives an upper limit $\sigma(\gamma p \to \rho' p;\ \rho' \to \eta\rho^o) < 28$ nb at the 68.3% confidence level. Combining this with the previously measured cross-sections for photoproduction of $\rho'(1600)$ decaying via $\rho^o\pi^+\pi^-$, $\rho^{\pm}\pi^{\mp}\pi^o$ and $\pi^+\pi^-$ [1-5], one obtains an upper limit for the branching ratio for $\rho'(1600) \to \eta\rho^o$ of 2%; this is to be compared with the value of 7 ± 2% which was estimated in $e^+e^- \to \eta\pi^+\pi^-$ from events having a $\pi^+\pi^-$ mass in the ρ^o mass range [7].

The signal in the $J^P = 3^-$ $A_2\pi$ state is consistent with the g(1690) meson which can be photoproduced diffractively, having C = -1 and $I^G = 1^+$. It is produced with a cross-section of 97 ± 28 ± 21 nb, corrected for the $A_2 \to \eta\pi$ branching ratio. Referring to the shape of the cos $\theta_{A_2\pi}$ distributions for the mass range of this signal (Fig. 12d), it may be noted that only $J^P = 3^-$ or 2^+ can give a peaking at cos $\theta_{A_2\pi} = 0$. Table 1 indicates that 3^- is favoured over 2^+ which, in any case, would be exotic. It should also be remarked that the distribution of cos $\theta_{A_2\pi}$ for $J^P = 1^-$ vanishes at cos $\theta_{A_2\pi} = 0$ thus ruling out any significant contribution from $\rho'(1600) \to A_2\pi$. On the assumption that the 3^- signal is due

solely to g(1690) production, the cross-sections for photoproduction of g(1690) in its other decay modes can be predicted from the known branching ratios [21]. One obtains

$$\sigma(\gamma p \to g p \; ; \quad g \to \pi^+\pi^-) = 51 \pm 22 \pm 11 \text{ nb}$$

$$\sigma(\gamma p \to g p \; ; \quad g \to \pi^+\pi^+\pi^-\pi^-) = 147 \pm 42 \pm 32 \text{ nb}$$

$$\sigma(\gamma p \to g p \; ; \quad g \to \rho^+\rho^-) = 18 \pm 16 \pm 4 \text{ nb} \; .$$

These values indicate that there could be a significant admixture of g(1690) contributing to the observed peaks seen in photoproduction of $\pi^+\pi^-$ and $\pi^+\pi^-\pi^+\pi^-$ which have been attributed to $\rho'(1600)$. The decay of g through $A_2\pi$ would also contribute in photoproduction of $\pi^+\pi^-\pi^0\pi^0$ [3]. In particular the cross-section for photoproduction of the 1.6 GeV peak in $\pi^+\pi^-$ is [5]:

$$(\gamma p \to \text{"}\rho'(1600)\text{"}p \; ; \quad \text{"}\rho'(1600)\text{"} \to \pi^+\pi^-) = 110 \pm 20 \text{ nb}$$

and no analysis has so far been done including a g(1690) contribution to the data. For $\rho^0\pi^+\pi^-$ photoproduction the cross-section is [1]:

$$(\gamma p \to \text{"}\rho'(1600)\text{"}p \; ; \quad \text{"}\rho'(1600)\text{"} \to \rho^0\pi^+\pi^-) = 540 \pm 170 \text{ nb}$$

so that again there may be a significant correction for g(1690) production.

5. CONCLUSIONS

Diffractively photoproduced $\eta\pi^+\pi^-$ states have been found to contain contributions from $\eta\rho^0$ and $A_2\pi$ substates. A Dalitz plot analysis has shown that the $\rho'(1600)$ is not an important component of the data and that there is a signal in $A_2\pi$ at a mass around 1.7 GeV which is consistent with the g meson.

Acknowledgements

We are grateful to the Omega Group at CERN for their help in running the spectrometer and providing on-line and off-line software. The work of the technical support staff in our home institutes, and the support at the computer centres at the Rutherford Appleton Laboratory, CERN, and the RHRZ at Bonn have been invaluable. We thank the SERC (UK), the BMFT (Fed. Rep. Germany), and the IN2P3 (France) for financial support.

REFERENCES

[1] H.H. Bingham et al., Phys. Lett. 41B (1972) 635.
D. Aston et al., Nucl. Phys. B189 (1981) 15.

[2] B. Esposito et al., Lett. Nuovo Cimento 28 (1980) 195.
C. Baggi et al., Phys. Lett. 95B (1980) 139.
A. Cordier et al., Phys. Lett. 109B (1982) 129.

[3] M. Atkinson et al., Zeitschrift f. Physik C26 (1985) 499.

[4] For a summary on e^+e^- results see for instance V. Sidorov, Proc. 1979 Int. Symp. on Lepton and Photon Interactions at High Energies (FNAL-Pub., Batavia, 1979), p. 490.

[5] D. Aston et al., Phys. Lett. 92B (1980) 215.
M.S. Atiya et al., Phys. Rev. Lett. 43 (1979) 1691.
K. Abe et al., Phys. Rev. Lett. 53 (1984) 751.

[6] D. Aston et al., Nucl. Phys. B174 (1980) 269.

[7] B. Delcourt et al., Phys. Lett. 113B (1982) 93.

[8] M. Atkinson et al., Nucl. Phys. B242 (1984) 269.

[9] J. Friedmann, Sage Reference Manual, SLAC Computational Group, Technical Memo 145 (1972).

[10] A.P. Waite, MAP Program Guide (1981), University of Manchester (unpublished).

[11] M. Atkinson et al., Phys. Lett. 138B (1984) 459.

[12] M. Ross and L. Stodolsky, Phys. Rev. 149 (1966) 1172.

[13] J.D. Jackson, Nuovo Cimento 34 (1964) 1644.

[14] K. Schilling, P. Seyboth and G. Wolf, Nucl. Phys. B15 (1970) 397.

[15] C. Zemach, Phys. Rev. 133 (1964) 1201.

[16] C. Zemach, Phys. Rev. 140 (1965) 97.

[17] C. Zemach, Phys. Rev. 140 (1965) 109.

[18] H. Marsiske, Diplomarbeit Bonn IR-84-38 (1984).

[19] M. Atkinson et al., Nucl. Phys. B231 (1984) 15.

[20] F. James and M. Roos, MINUIT Computer Physics Communications 10 (1975) 343.

[21] Review of Paricle Properties, Particle Data Group, Rev. Mod. Phys. 56 (1984).

Table 1

Percentages of various spin-parity contributions to the $\eta\pi^+\pi^-$ system in the mass range 1.5 to 1.7 GeV as obtained by fits to the Dalitz plot. Each column corresponds to a single fit and the symbol "~" means that the particular contribution was constrained to be zero.

Spin-parity state	Final fit		Other fits			
1^- $\eta\rho$	$17.1^{+6.8}_{-8.3}$	$13.0^{+7.4}_{-7.3}$	$18.8^{+6.4}_{-6.8}$	$24.7^{+5.4}_{-7.2}$	$24.5^{+5.4}_{-7.2}$	~
$\eta\rho$ phase space	$2.6^{+9.3}_{-2.6}$	$6.1^{+9.0}_{-5.6}$	$3.1^{+8.7}_{-3.1}$	$0.1^{+6.6}_{-0.1}$	$0.1^{+8.0}_{-0.1}$	$22.9^{+6.1}_{-6.0}$
1^- $A_2\pi$	~	~	~	$4.8^{+5.5}_{-4.8}$	~	~
2^+ $A_2\pi$	~	~	$19.1^{+6.1}_{-5.0}$	~	~	~
3^- $A_2\pi$	$17.3^{+5.5}_{-5.4}$	$23.2^{+4.8}_{-4.7}$	~	~	~	~
$A_2\pi$ phase space	$12.0^{+5.9}_{-5.8}$	~	$8.3^{+7.3}_{-6.9}$	$20.0^{+6.5}_{-3.1}$	$23.8^{+4.7}_{-5.0}$	$23.4^{+5.2}_{-5.1}$
$\eta\pi\pi$ phase space	$51.1^{+7.2}_{-7.0}$	$57.9^{+6.6}_{-6.6}$	$50.9^{+7.3}_{-4.1}$	$50.6^{+7.0}_{-6.8}$	$51.8^{+6.6}_{-3.1}$	$53.9^{+7.6}_{-7.5}$
Negative log-likelihood value	2546.27	2548.57	2548.32	2551.49	2551.91	2556.30

Table 2

Cross-sections as a function of the $\eta\pi\pi$ mass (nb/200 MeV)

	$\eta\pi^-\pi^+$ mass range (GeV)					
Spin-parity state	1.00–1.20	1.20–1.40	1.40–1.60	1.60–1.80	1.80–2.00	2.00–2.40
1^- $\eta\rho$	$1.0^{+2.3}_{-1.0}$	$21.7^{+4.1}_{-4.1}$	$10.7^{+4.9}_{-4.9}$	$8.0^{+4.2}_{-4.4}$	$1.0^{+1.8}_{-1.0}$	$1.0^{+1.0}_{-1.0}$
$\eta\rho$ phase space	$1.6^{+2.1}_{-1.6}$	$8.7^{+3.3}_{-3.2}$	$9.9^{+5.2}_{-5.1}$	$7.2^{+5.5}_{-5.0}$	$7.9^{+2.0}_{-2.0}$	$5.3^{+1.4}_{-1.3}$
3^- $A_2\pi$	--	--	$3.6^{+2.6}_{-2.6}$	$8.9^{+3.2}_{-3.0}$	$1.8^{+2.0}_{-1.8}$	$1.0^{+1.6}_{-1.0}$
$A_2\pi$ phase space	--	--	$3.3^{+2.4}_{-2.3}$	$8.2^{+4.1}_{-3.8}$	$1.8^{+1.0}_{-1.0}$	$4.9^{+1.7}_{-1.7}$
$\eta\pi\pi$ phase space	$13.1^{+2.2}_{-2.5}$	$24.2^{+4.0}_{-4.8}$	$25.1^{+4.9}_{-4.8}$	$24.2^{+3.8}_{-3.7}$	$31.1^{+2.9}_{-2.6}$	$18.0^{+2.2}_{-2.2}$

Figure captions

Fig. 1 : $\gamma\gamma$ mass spectrum for $\eta\pi^+\pi^-$ events having ΔE (see text) between -1.5 and +2.5 GeV.

Fig. 2 : Missing energy, ΔE, for $\eta\pi^+\pi^-$ events obtained by a peak minus wings subtraction on the η signal.

Fig. 3 : Mass spectrum of $\eta\pi^+\pi^-$ (raw data). The curve shows the acceptance.

Fig. 4 : a) $\eta\pi^\pm$ mass spectrum for all events.
b) $\eta\pi^\pm$ mass spectrum showing a fit as described in the text.

Fig. 5 : Cross-section for $A_2^\pm$ production as a function of the $\eta\pi^+\pi^-$ mass obtained from fits to the $\eta\pi^\pm$ mass spectra.

Fig. 6 : a) $\pi^+\pi^-$ mass spectrum for all events.
b) $\pi^+\pi^-$ mass spectrum showing a fit as described in the text.

Fig. 7 : Cross-section for ρ^0 production as a function of the $\eta\pi^+\pi^-$ mass obtained from fits to the $\pi^+\pi^-$ mass spectra.

Fig. 8 : Normalized spherical harmonic moments of the $\eta\pi^+\pi^-$ decay distribution in the s-channel helicity system.

Fig. 9 : Cross-section for production of various spin-parity states obtained from fits to the Dalitz plot.

Fig. 10 : $\eta\pi^\pm$ mass spectra for bins of $\eta\pi^+\pi^-$ mass. The open points are the data and the full points are the results of the Dalitz plot fits.

Fig. 11 : $\pi^+\pi^-$ mass spectra for bins of $\eta\pi^+\pi^-$ mass. The open points are the data and the full points are the results of the Dalitz plot fits.

Fig. 12 : Distributions of cos $\theta_{A_2\pi}$, the angle between the $\pi^{\pm}$ direction and the η in the $\eta\pi$ rest frame, for bins of $\eta\pi^+\pi^-$ mass. The open points are the data and the full points are the results of the Dalitz plot fits.

Fig. 13 : Distributions of cos $\theta_{\eta\rho}$, the angle between the η and the π^+ directions in the $\pi^+\pi^-$ rest frame, for bins of $\eta\pi^+\pi^-$ mass. The open points are the data and the full points are the results of the Dalitz plot fits.

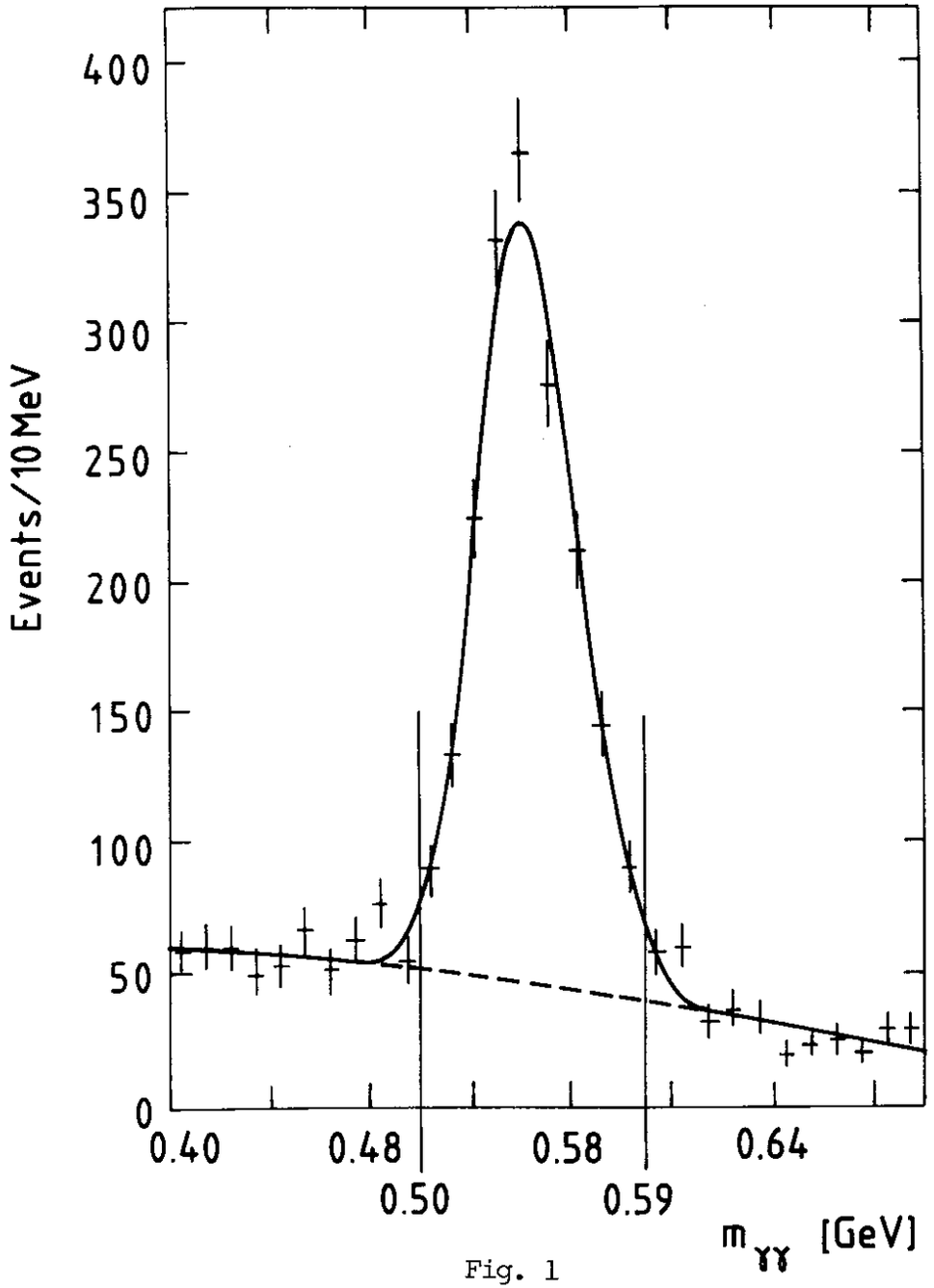
Events/10 MeV
400
350
300
250
200
150
100
50
0
0.40
0.48
0.50
0.58
0.59
0.64
$m_{\gamma\gamma}$ [GeV]

Fig. 1

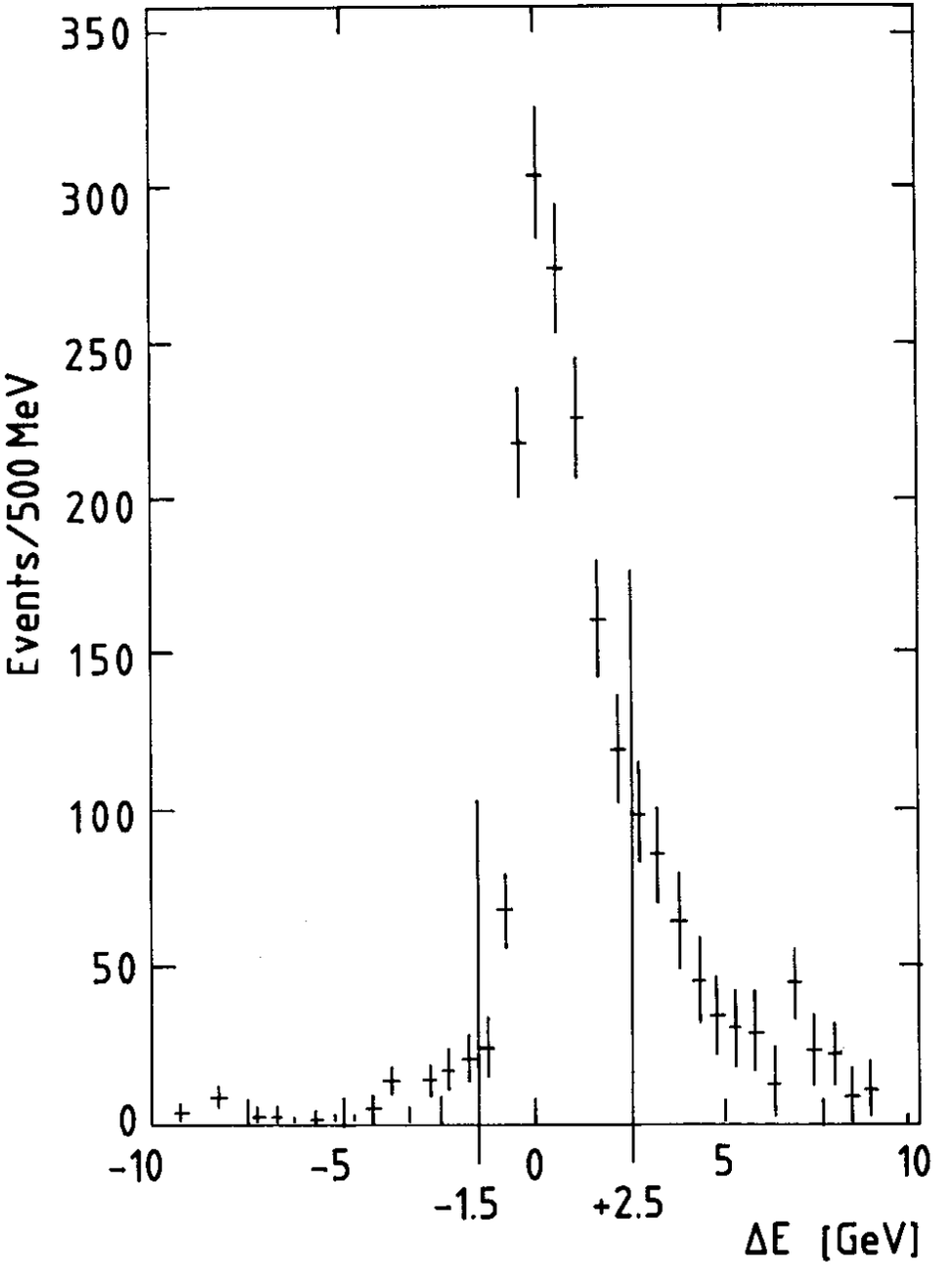
Events/500 MeV
350
300
250
200
150
100
50
0
-10
-5
-1.5
0
+2.5
5
10
ΔE [GeV]

Fig. 2

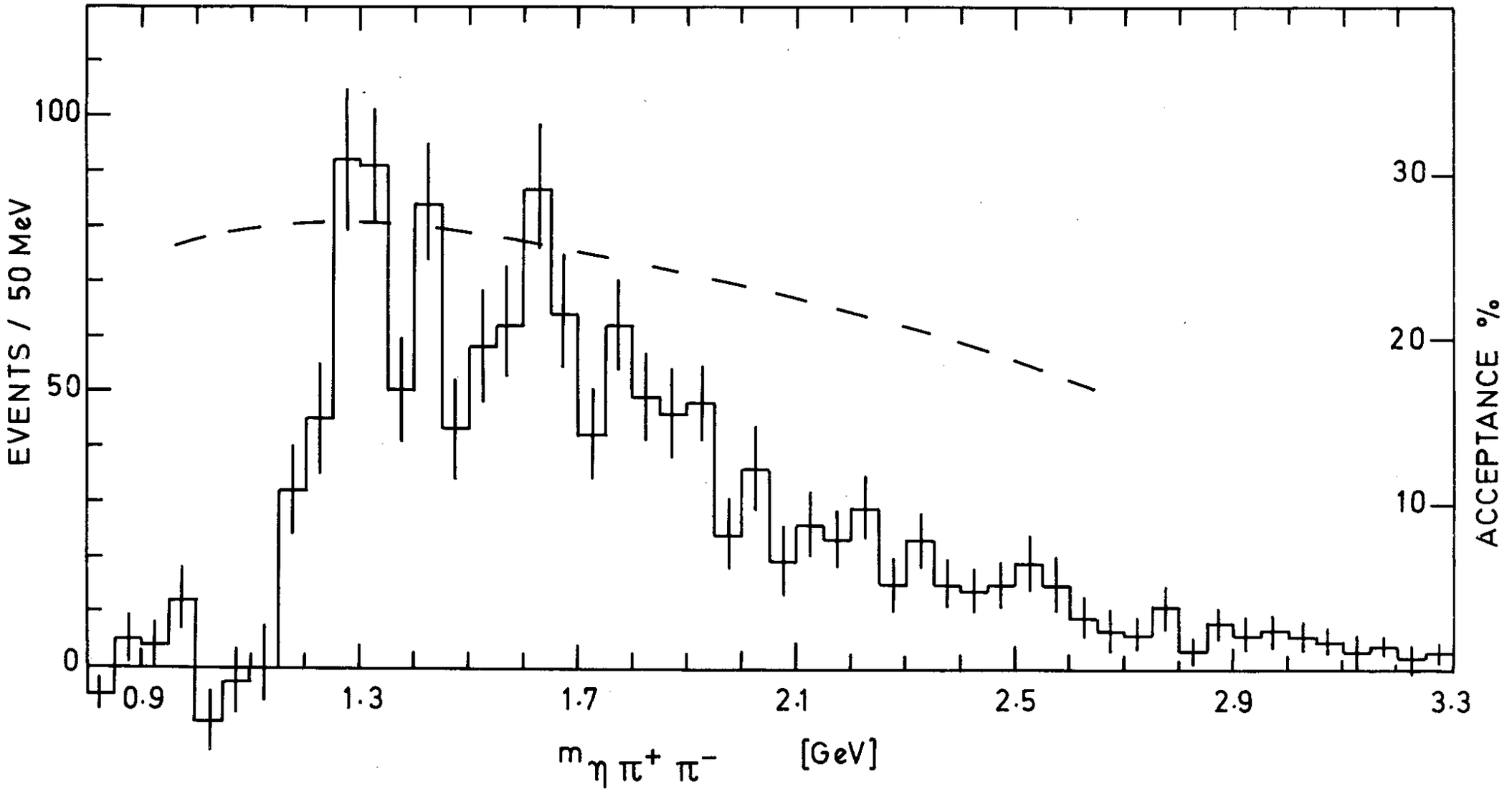
EVENTS / 50 MeV
100
50
0
0.9
1.3
1.7
2.1
2.5
2.9
3.3
$m_{\eta\,\pi^+\,\pi^-}$ [GeV]
30
20
10
ACCEPTANCE %

Fig. 3

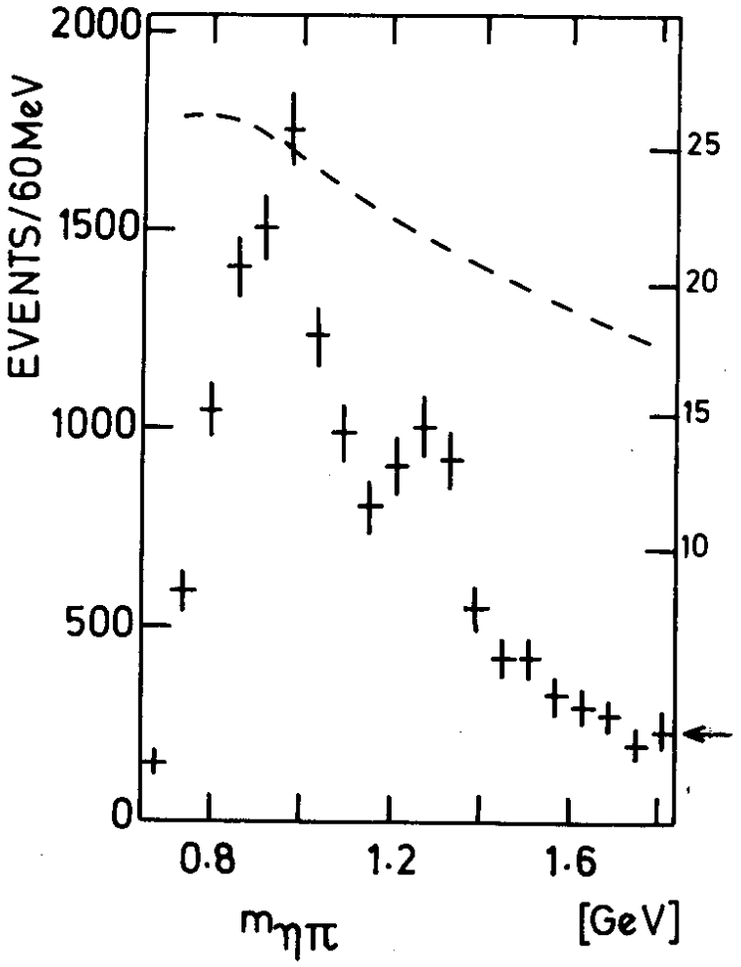

Fig. 4a

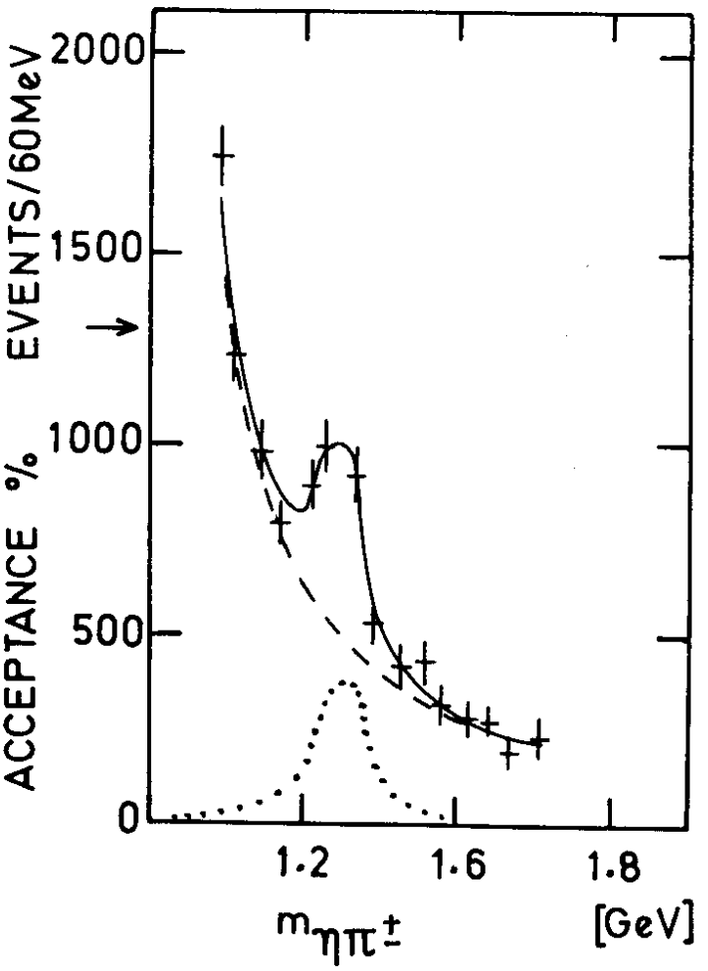

Fig. 4b

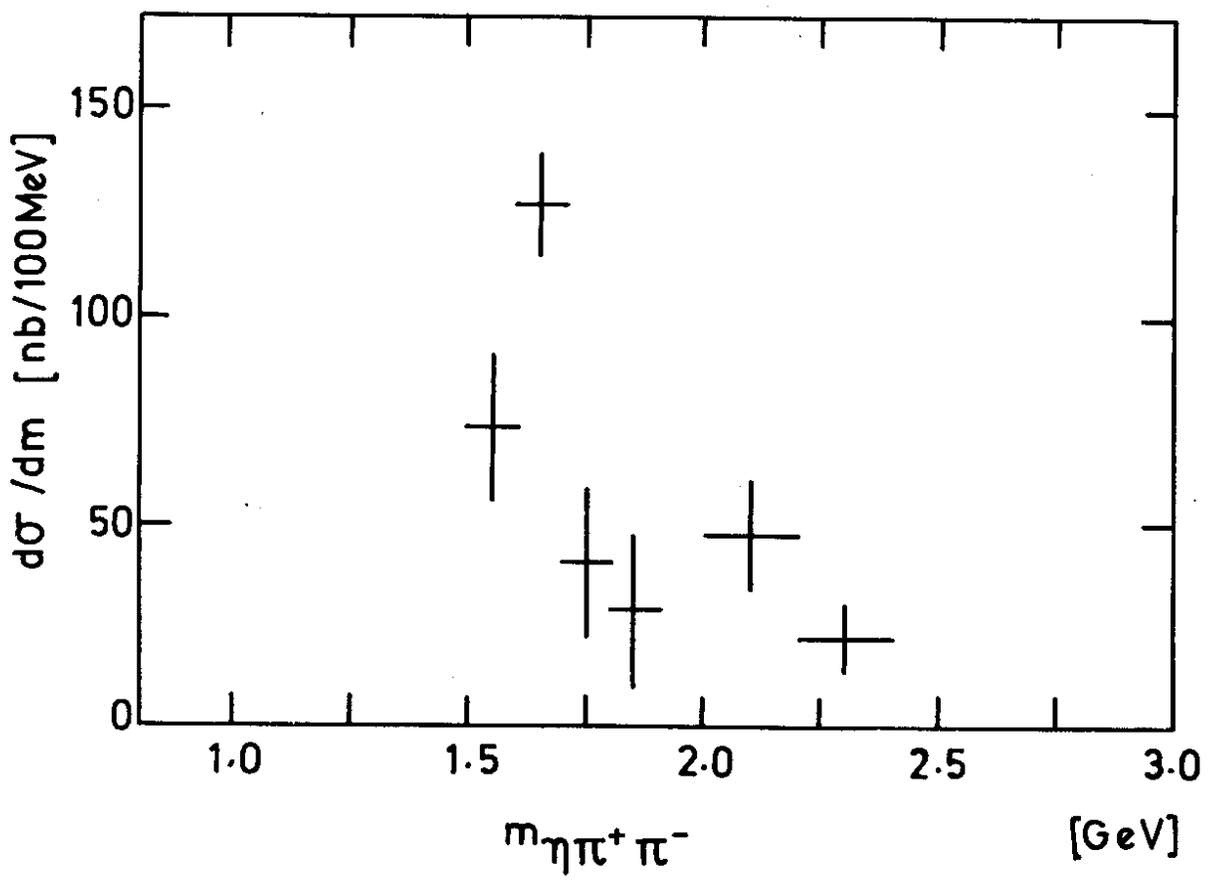

Fig. 5

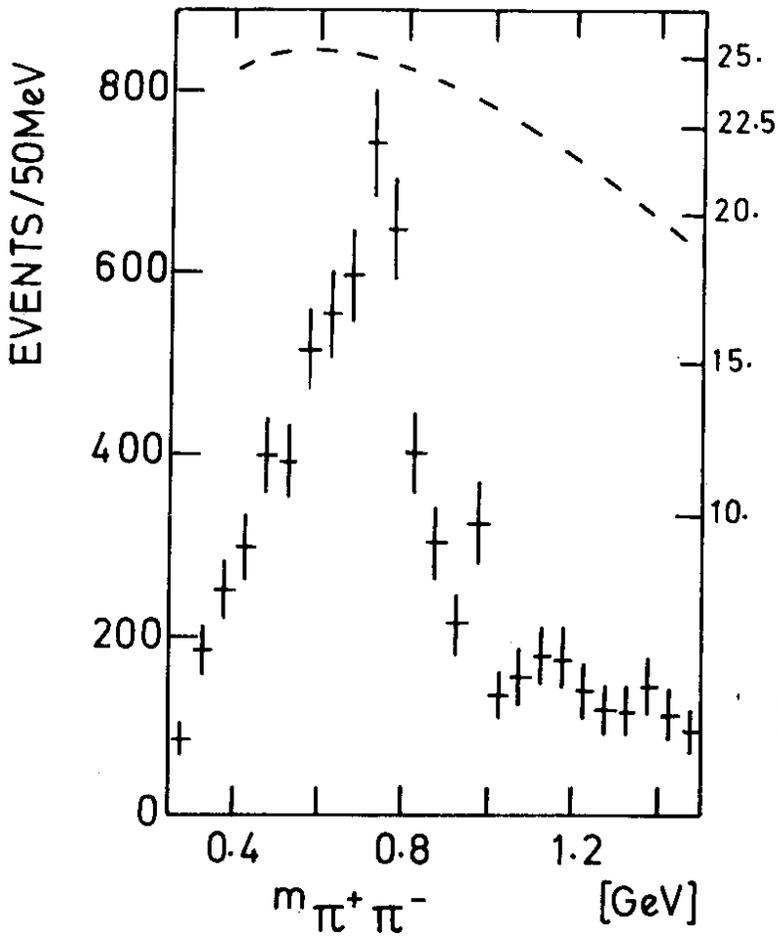

Fig. 6a

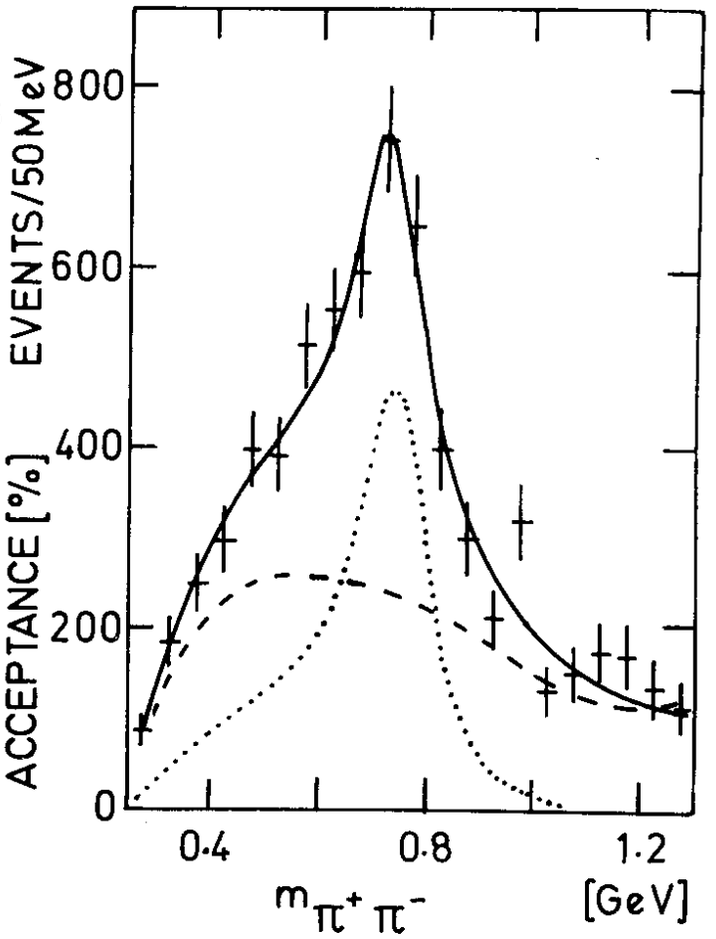

Fig. 6b

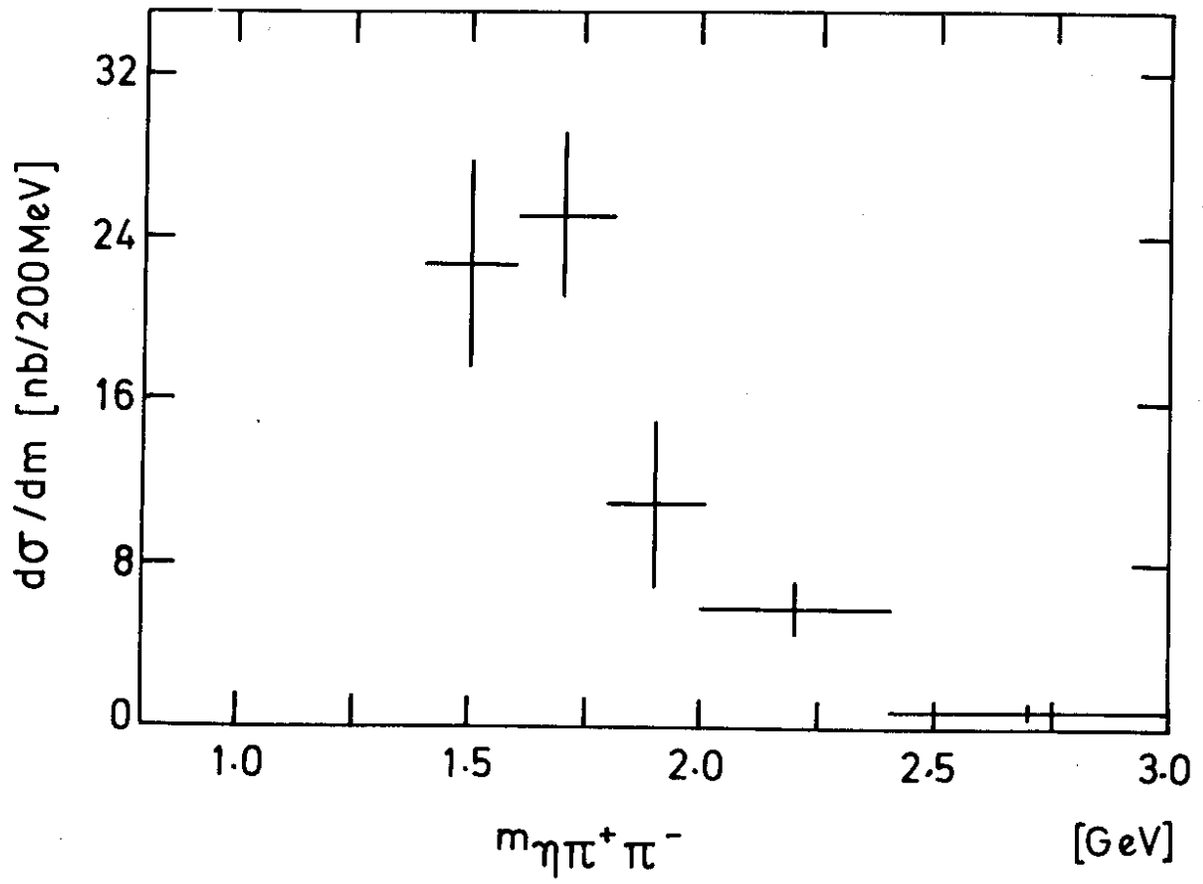

Fig. 7

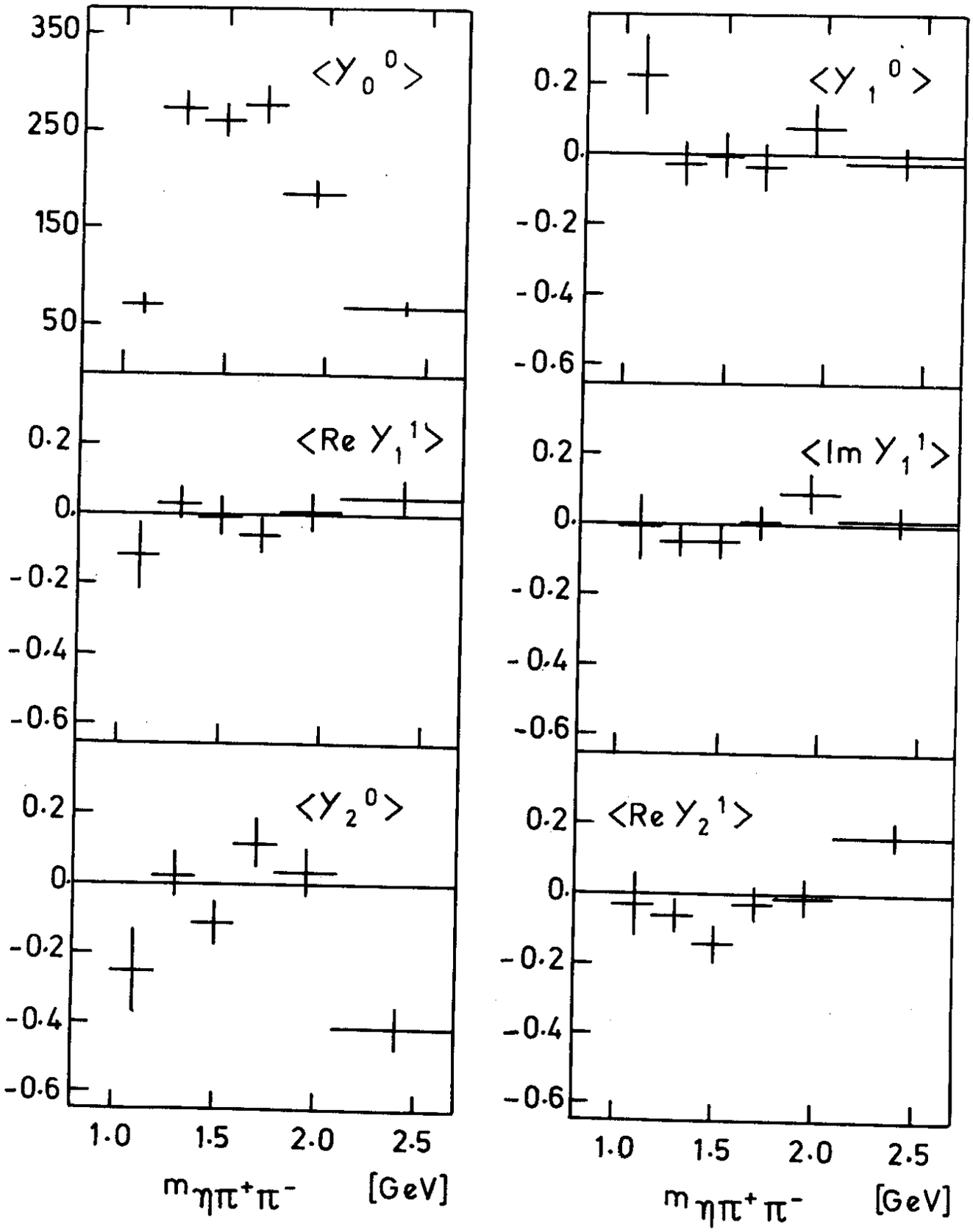
350
250
150
50
$\langle Y_0^0 \rangle$
0.2
0.
-0.2
-0.4
-0.6
$\langle \mathrm{Re}\, Y_1^1 \rangle$
0.2
0.
-0.2
-0.4
-0.6
$\langle Y_2^0 \rangle$
1.0
1.5
2.0
2.5
$m_{\eta\pi^+\pi^-}$ [GeV]
0.2
0.
-0.2
-0.4
-0.6
$\langle Y_1^0 \rangle$
0.2
0.
-0.2
-0.4
-0.6
$\langle \mathrm{Im}\, Y_1^1 \rangle$
0.2
0.
-0.2
-0.4
-0.6
$\langle \mathrm{Re}\, Y_2^1 \rangle$
1.0
1.5
2.0
2.5
$m_{\eta\pi^+\pi^-}$ [GeV]

Fig. 8

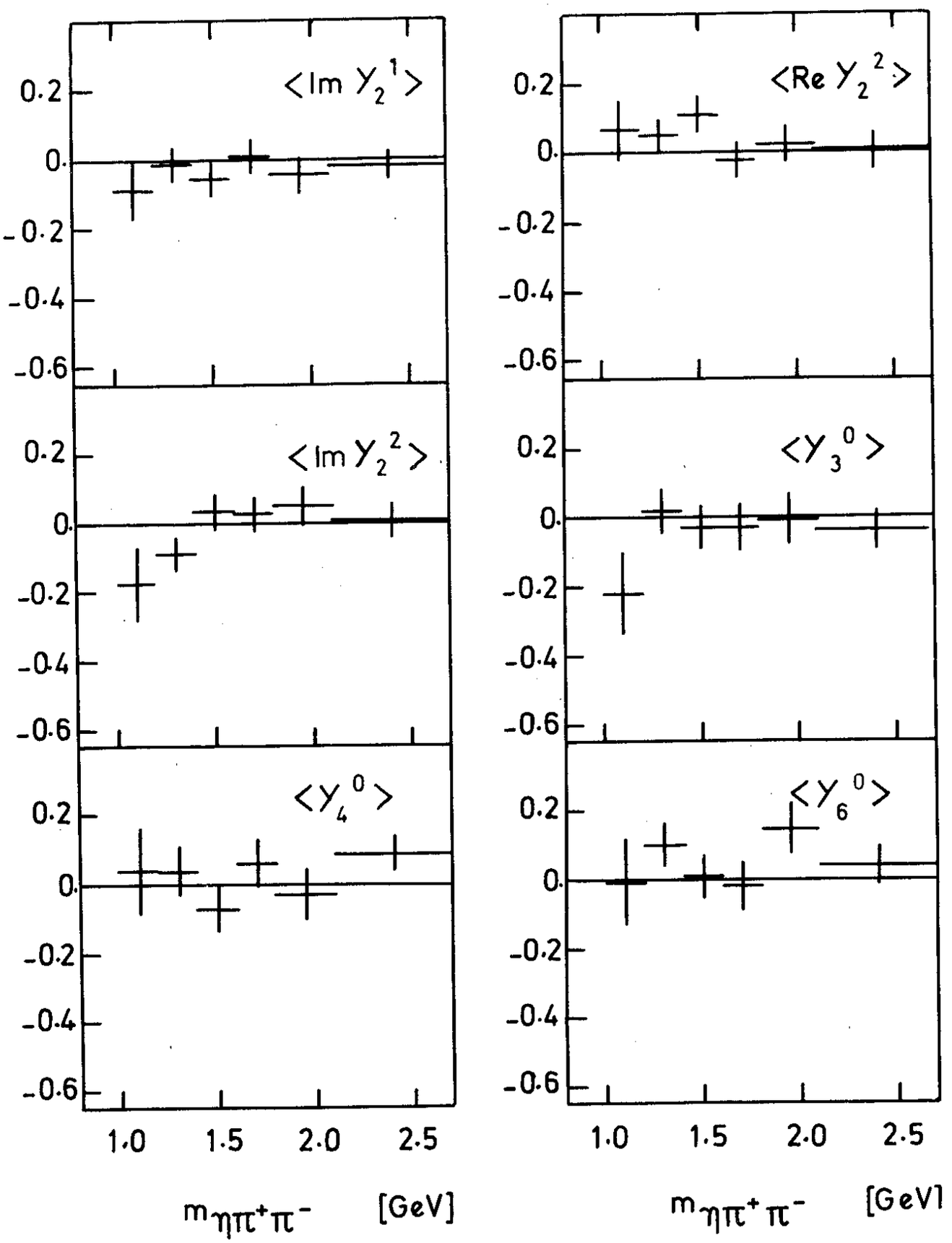

Fig. 8 (continued)

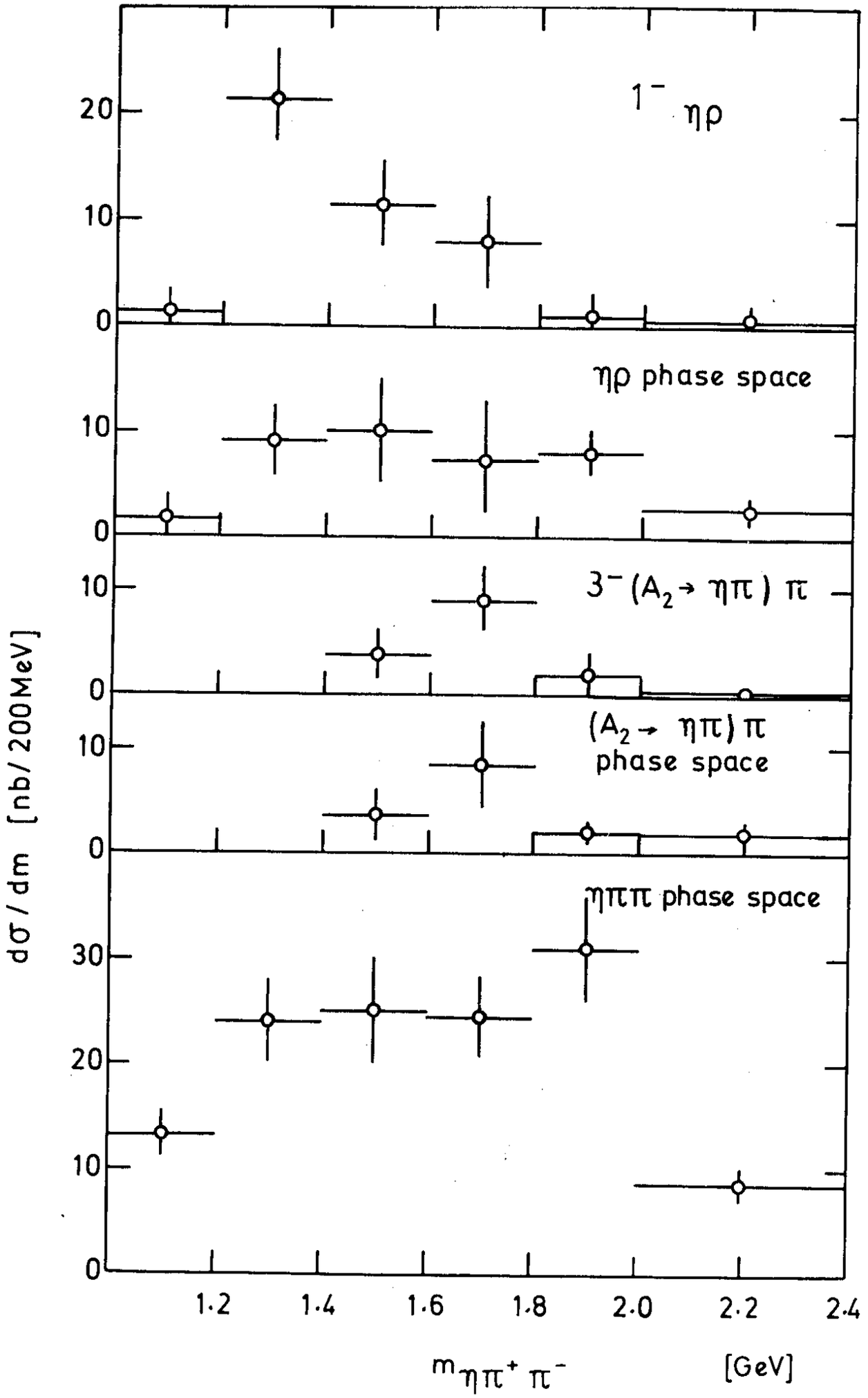
1^- ηρ
ηρ phase space
3^- ($A_2 \to \eta\pi$) π
($A_2 \to \eta\pi$) π phase space
ηππ phase space
dσ/dm [nb/200MeV]
$m_{\eta\pi^+\pi^-}$ [GeV]
0
10
20
30
1.2
1.4
1.6
1.8
2.0
2.2
2.4

Fig. 9

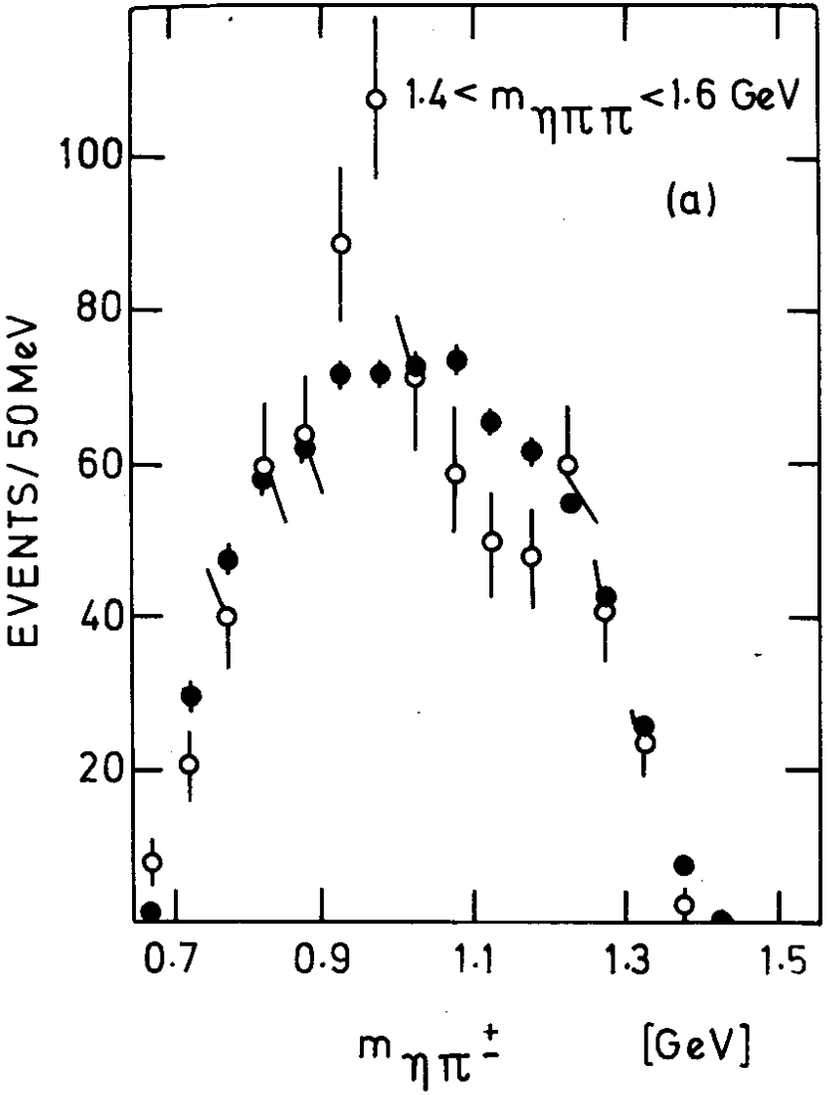

Fig. 10a

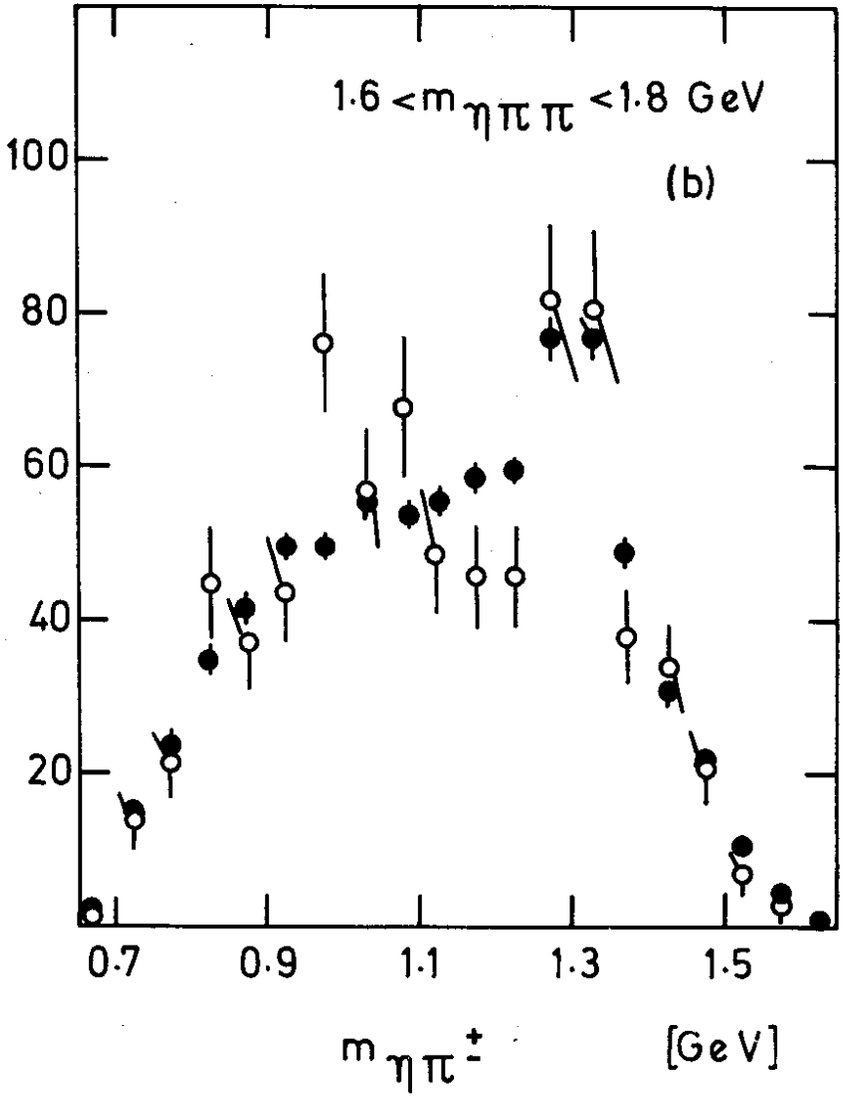

Fig. 10b

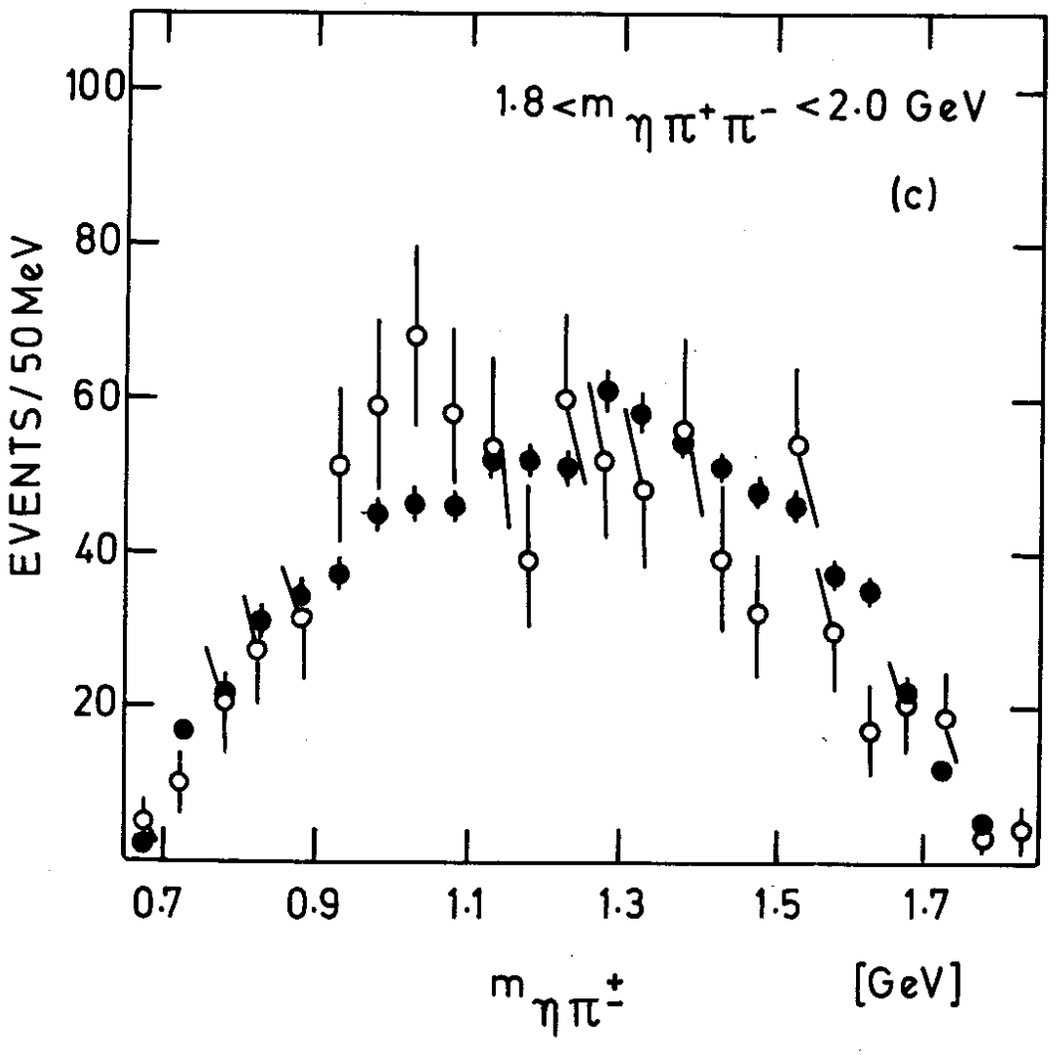
1·8<m η π+ π- <2·0 GeV
(c)
EVENTS/50 MeV
100
80
60
40
20
0·7
0·9
1·1
1·3
1·5
1·7
m η π±
[GeV]

Fig. 10c

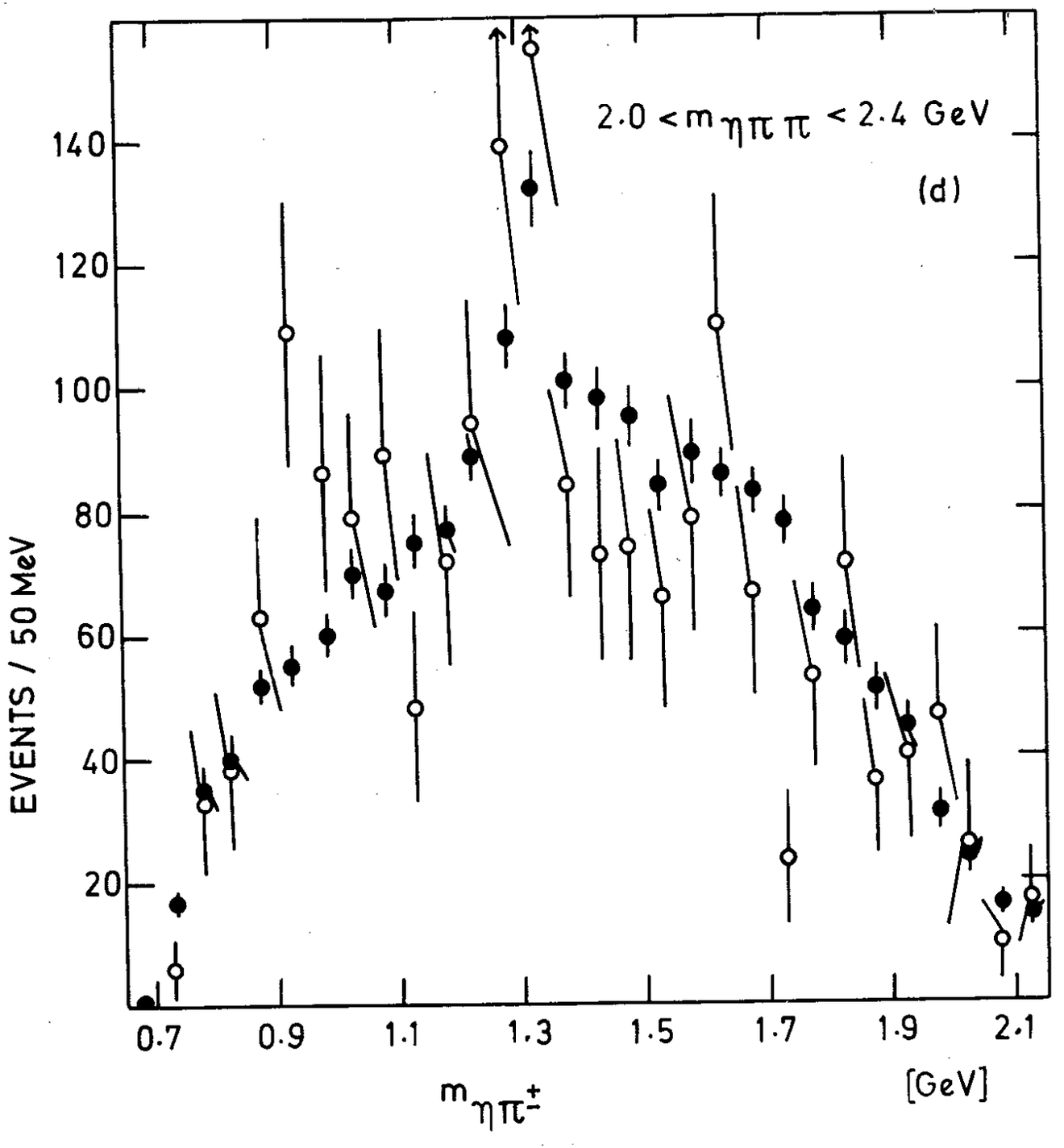
2.0 < m ηππ < 2.4 GeV
(d)
EVENTS / 50 MeV
140
120
100
80
60
40
20
0.7
0.9
1.1
1.3
1.5
1.7
1.9
2.1
m ηπ±
[GeV]

Fig. 10d

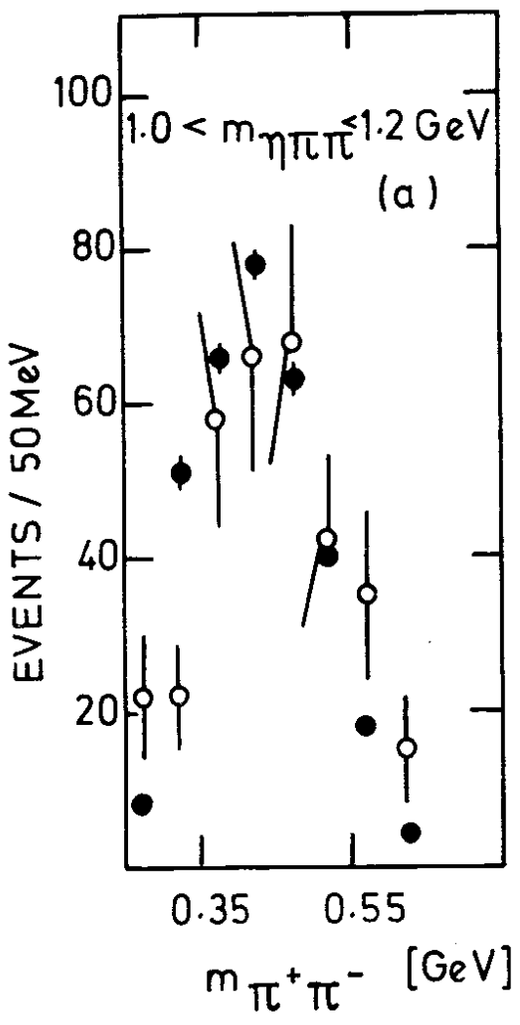

Fig. 11a

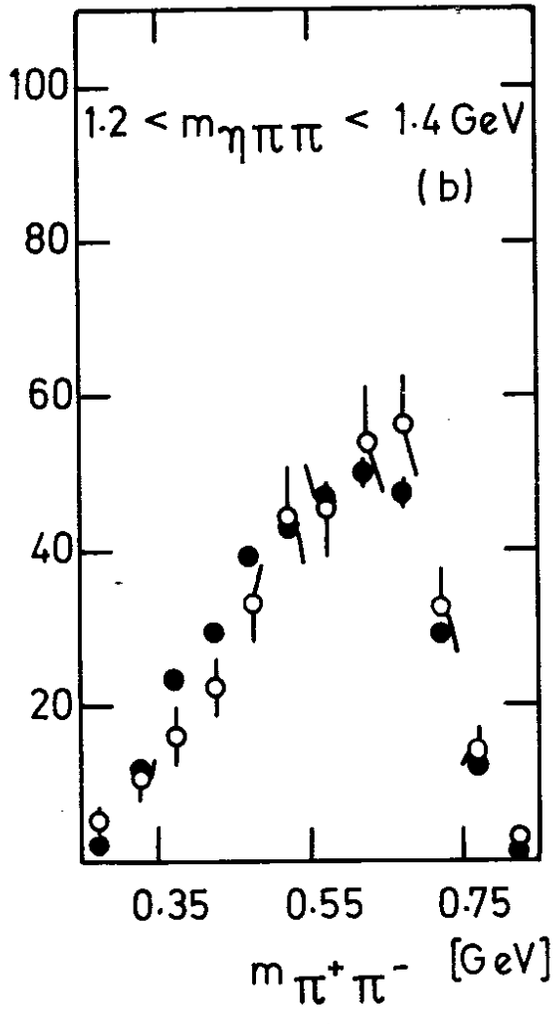

Fig. 11b

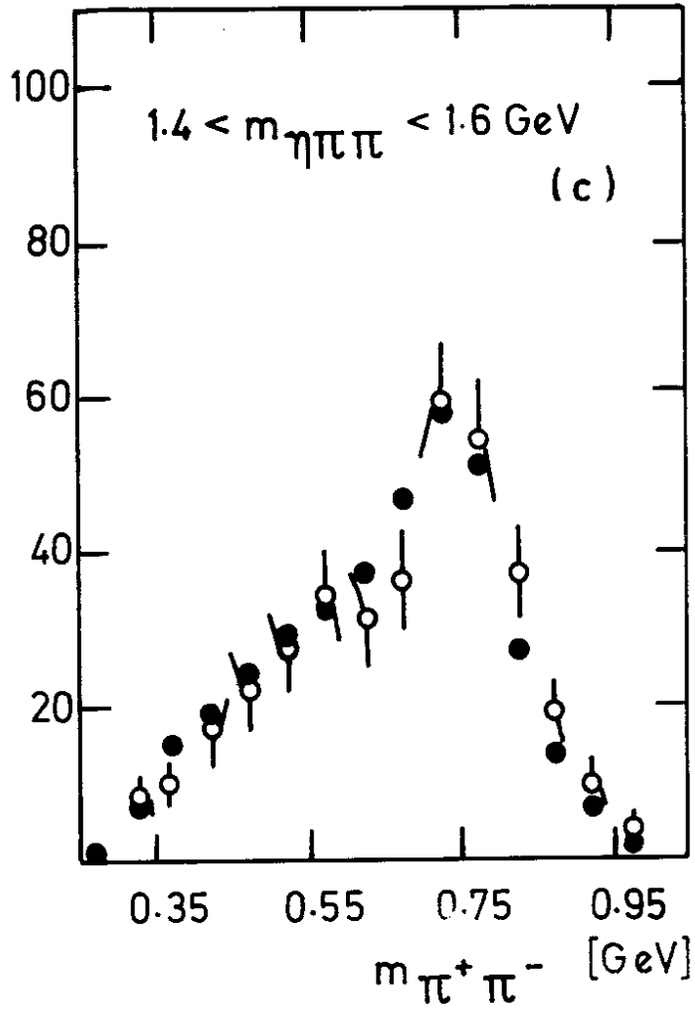

Fig. 11c

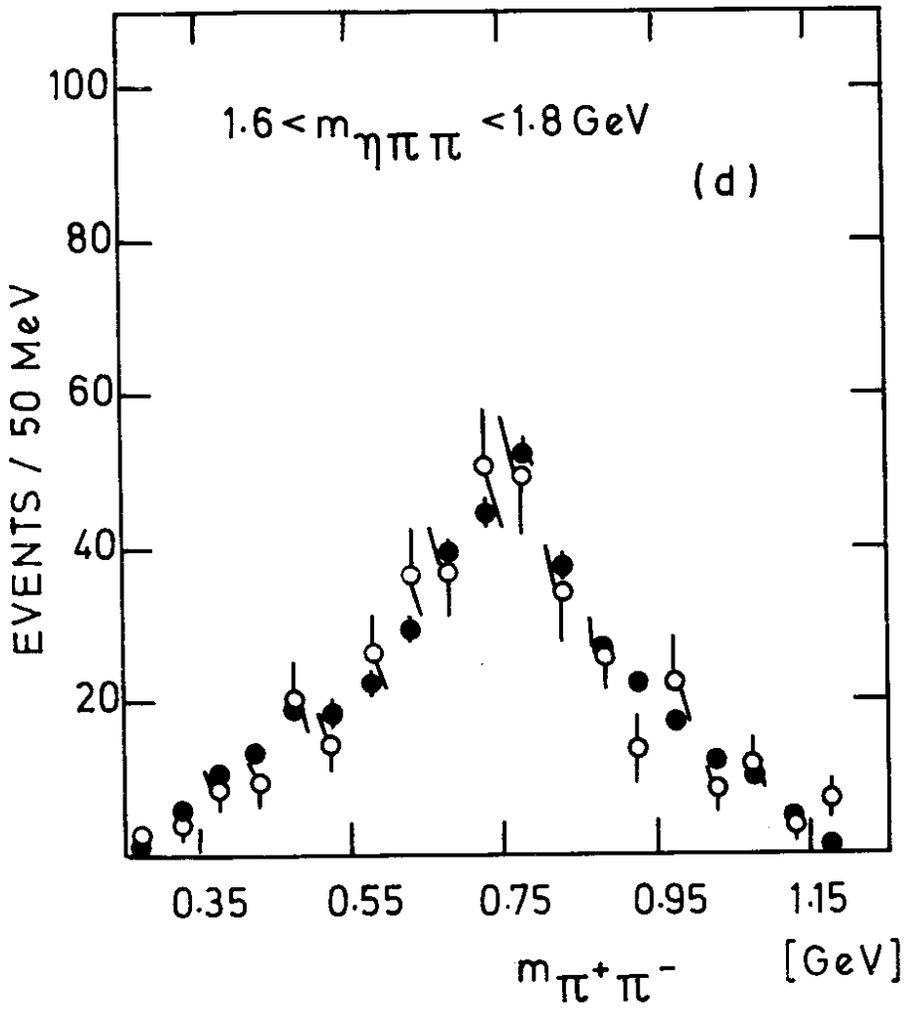

Fig. 11d

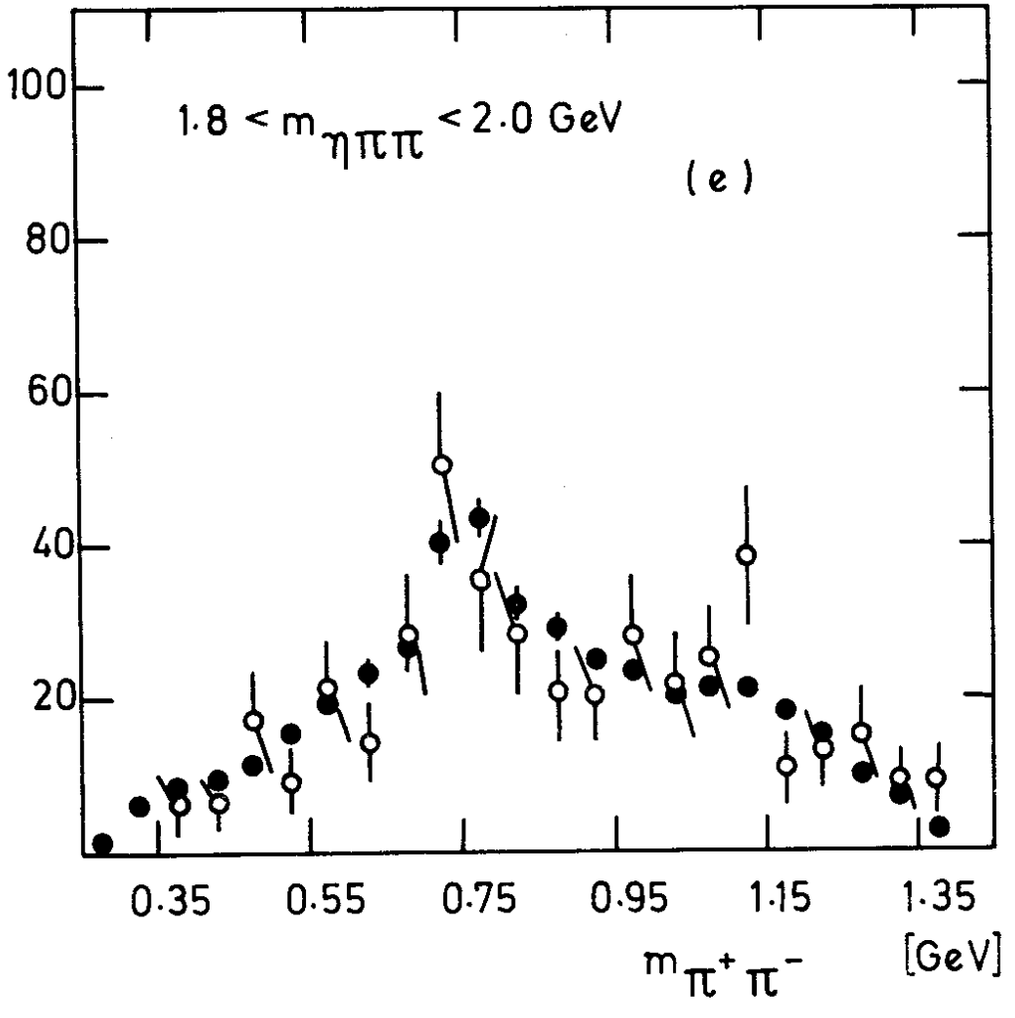

Fig. 11e

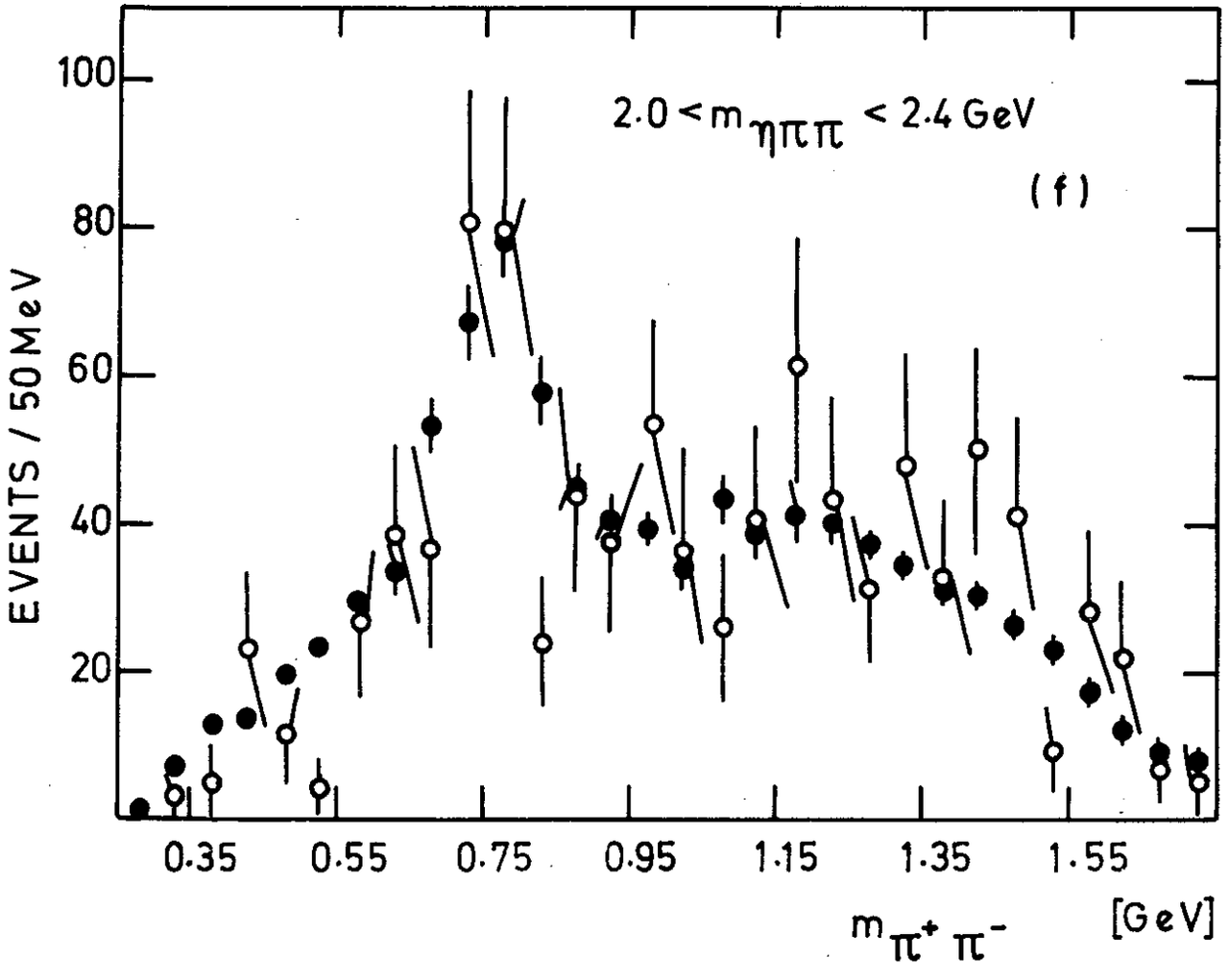
100
80
60
40
20
EVENTS / 50 MeV
2.0 < m ηππ < 2.4 GeV
(f)
0.35
0.55
0.75
0.95
1.15
1.35
1.55
m π+ π-
[GeV]

Fig. 11f

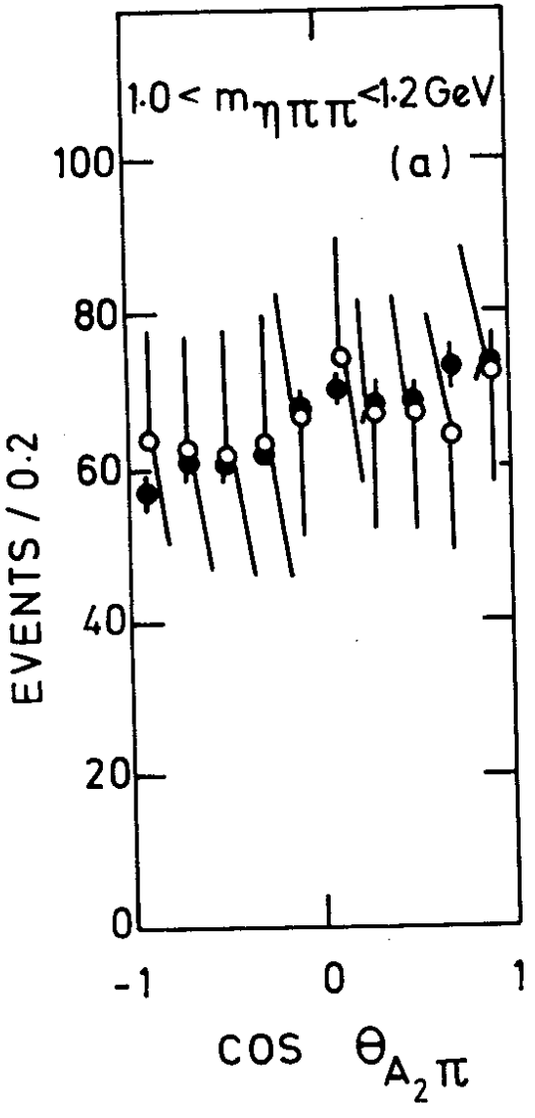

Fig. 12a

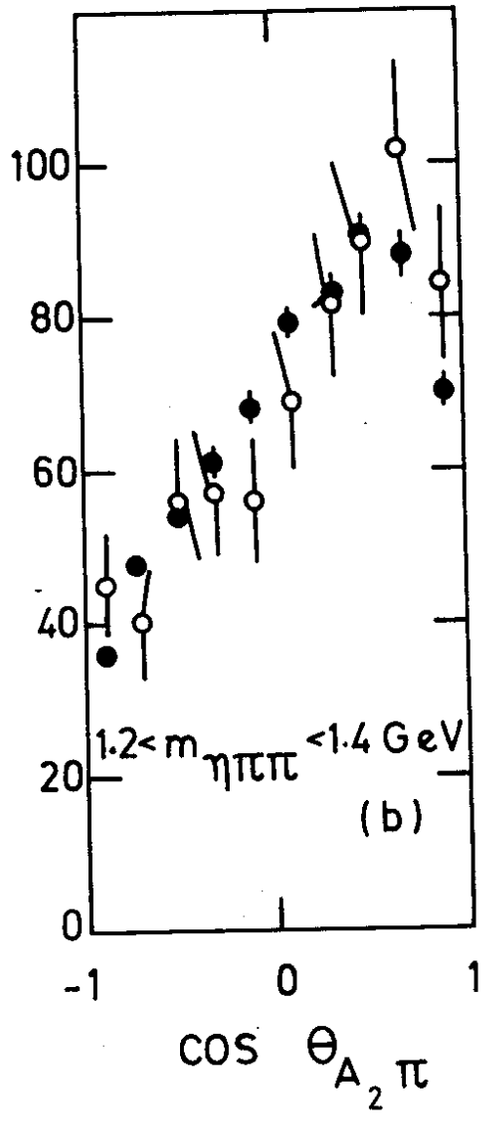

Fig. 12b

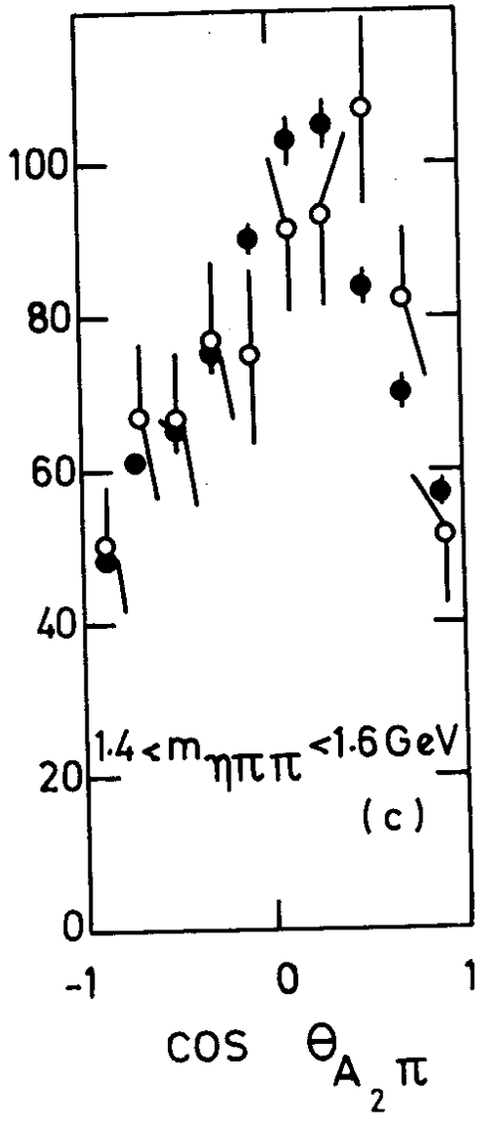

Fig. 12c

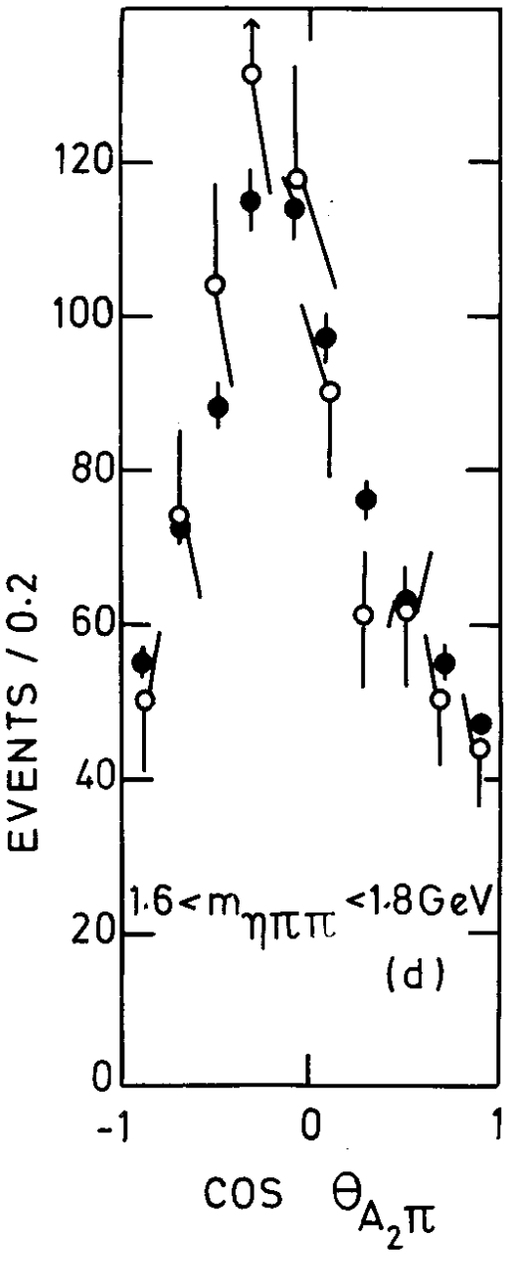

Fig. 12d

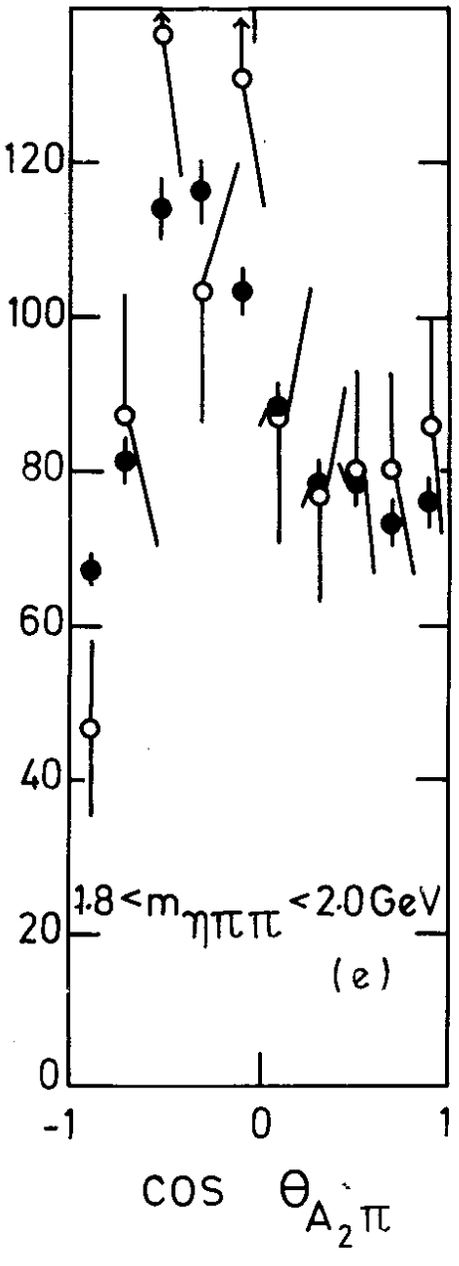

Fig. 12e

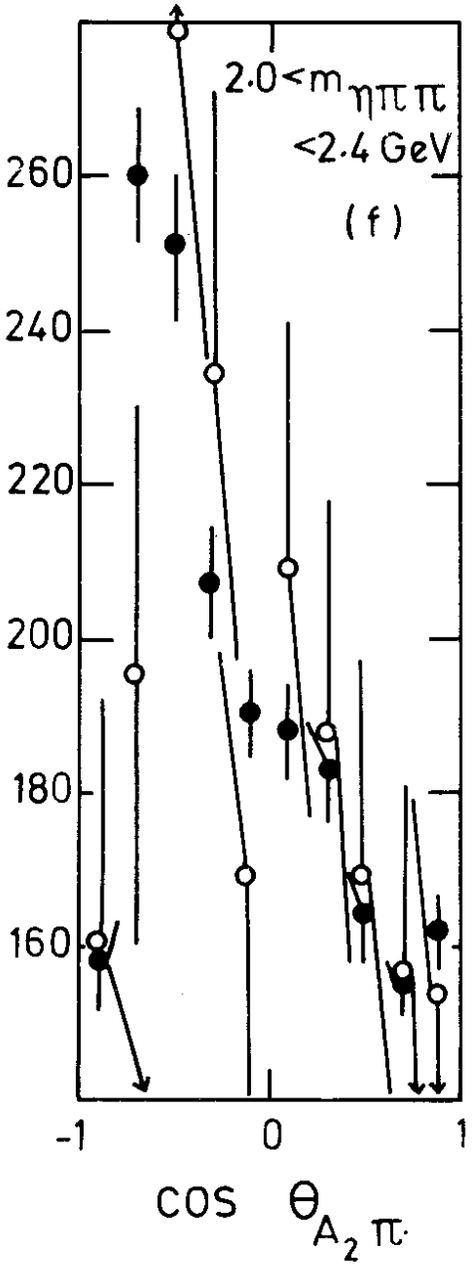

Fig. 12f

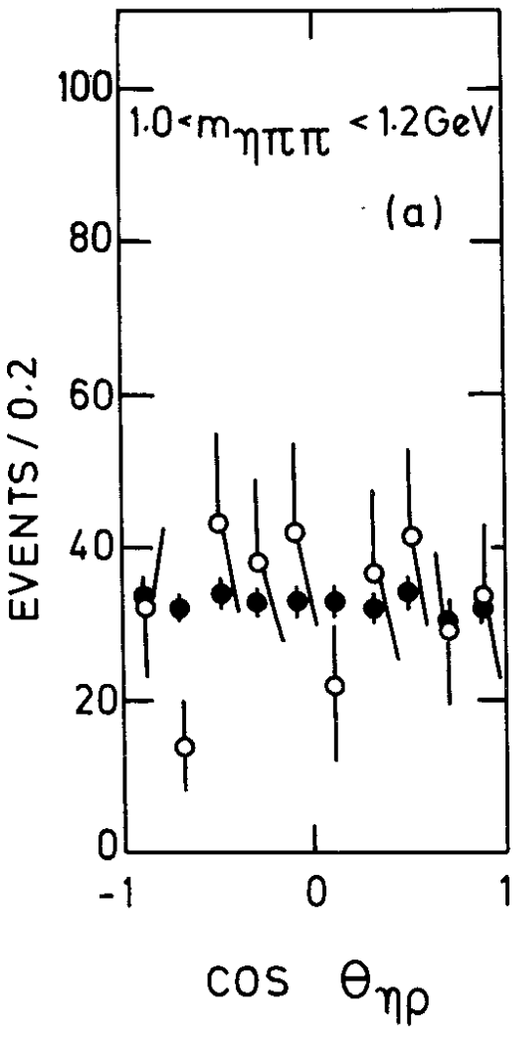

Fig. 13a

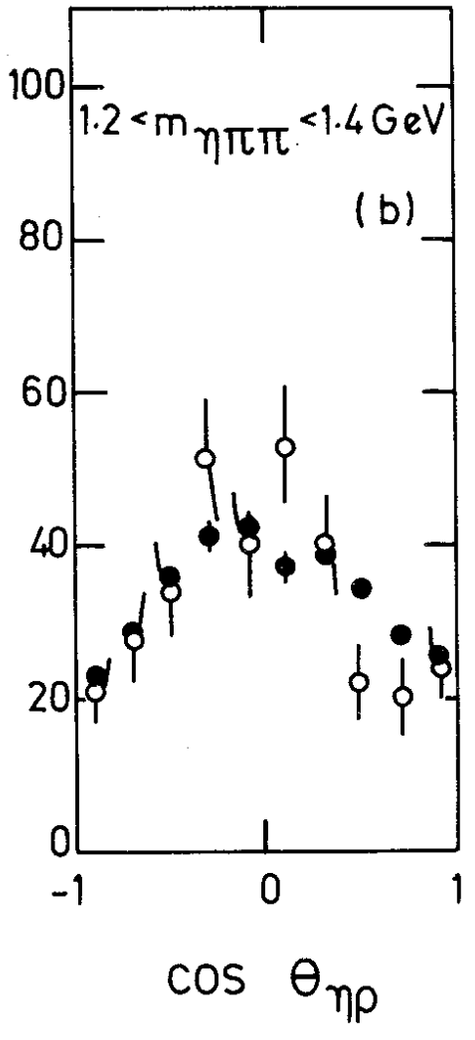

Fig. 13b

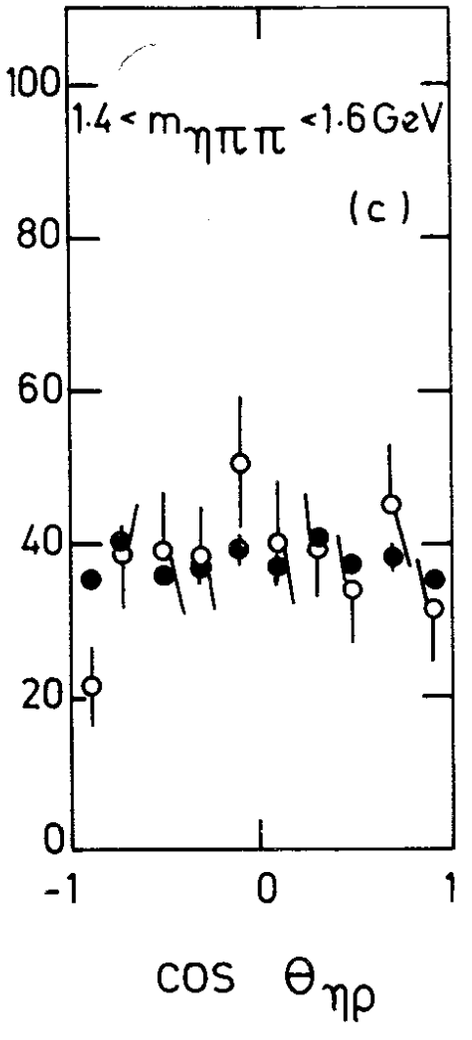

Fig. 13c

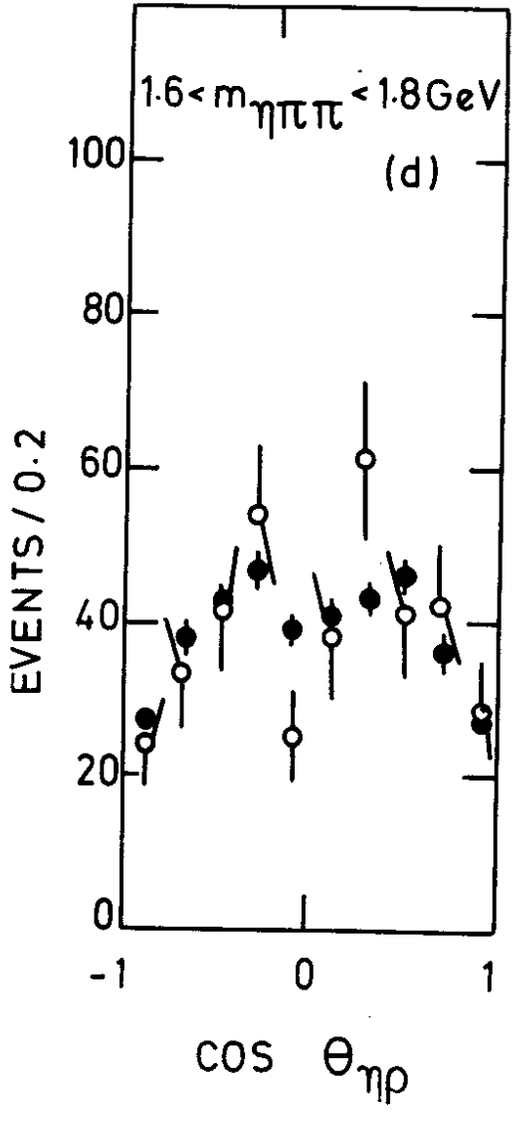

Fig. 13d

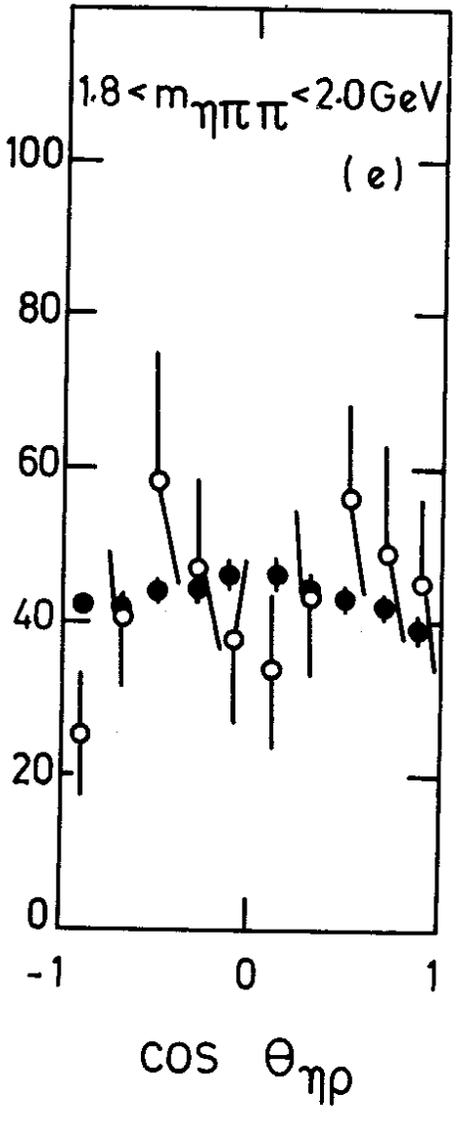

Fig. 13e

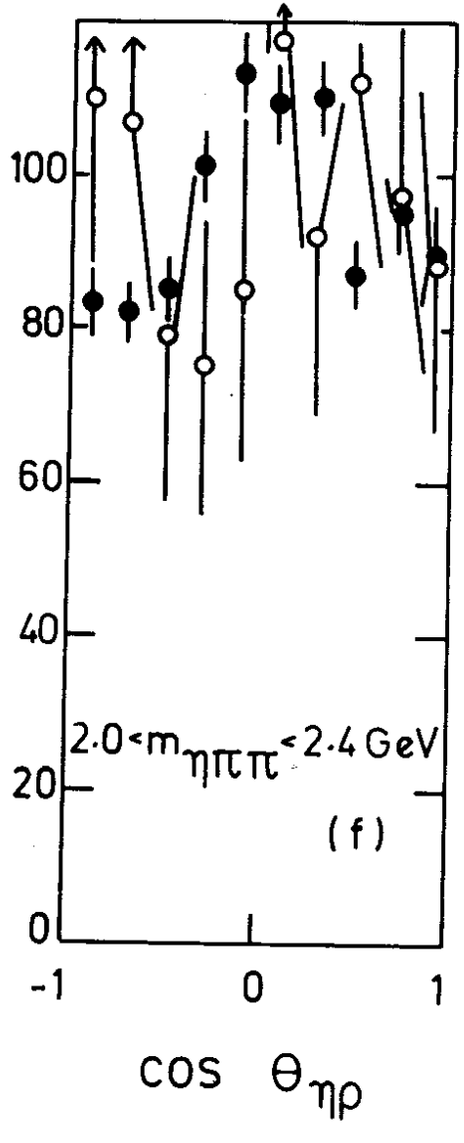

Fig. 13f